Title: A multiscale approach to investigate fluorescence and NDVI imaging as proxy of photosynthetic traits in wheat

Running title: Multi-scale imaging and photosynthesis phenotyping in wheat

Nicolas Virlet[1†*], João Paulo Pennacchi[1,2†], Pouria Sadeghi-Tehran[1], Tom Ashfield[1,3], Douglas J. Orr[4], Elizabete Carmo-Silva[4], Malcolm J. Hawkesford[1]

†These authors contributed equally to this work

[1]Sustainable Soils and Crops, Rothamsted Research, West Common, Harpenden, AL5 2JQ, UK

Email: nicolas.virlet@rothamsted.ac.uk, Pouria.Sadeghi-Tehran@syngenta.com, malcolm.hawkesford@rothamsted.ac.uk

[2]Department of Biology, Universidade Federal de Lavras, Aquenta Sol, Lavras, 37200-000, Brazil

Email: jppennacchi@gmail.com

[3]Crop Health and Protection, Rothamsted Research, West Common, Harpenden, AL5 2JQ, UK

tom.ashfield@rothamsted.ac.uk

[4]Lancaster Environment Centre, Lancaster University, Library Avenue, Lancaster, LA1 4YQ, UK

Email : e.carmosilva@lancaster.ac.uk, d.j.orr@lancaster.ac.uk

*Correspondence : nicolas.virlet@rothamsted.ac.uk

Date of submission : 10/11/2013

Number of tables and figures: five tables and three figures

Number of supplementary data: five tables and seven figures

Word count: 6231

Highlight: A temporal and multi-scale study of fluorescence and NDVI imaging used as a proxy for photosynthetic parameters

ABSTRACT

With the development of the digital phenotyping, repeated measurements of agronomic traits over time are easily accessible, notably for morphological and phenological traits. However high throughput methods for estimating physiological traits such as photosynthesis are lacking. This study demonstrates the links of fluorescence and reflectance imaging with photosynthetic traits. Two wheat cultivars were grown in pots in a controlled environment. Photosynthesis was characterised by gas-exchange and biochemical analysis at five time points, from booting to 21 days post anthesis. On the same days imaging was performed on the same pots, at leaf and plant scale, using indoor and outdoor phenotyping platforms, respectively. Five image variables (F_v/F_m and NDVI at the whole plant level and F_v/F_m, $\Phi(II)_{532}$ and $\Phi(NPQ)_{1077}$ at the leaf scale) were compared to variables from A-Ci and A-Par curves, biochemical analysis, and fluorescence instruments. The results suggested that the image variables are robust estimators of photosynthetic traits, as long as senescence is driving the variability. Despite contrasting cultivar behaviour, linear regression models which account for the cultivar and the interaction effects, further improved the modelling of photosynthesis indicators. Finally, the results highlight the challenge of discriminating functional to cosmetic stay green genotypes using digital imaging.

Keywords: Rubisco, gas-exchange, chlorophyll fluorescence, phenotyping, crop physiology, leaf to whole plant, stay-green, *Triticum aestivum*,

Abbreviations:

V_{cmax}: maximum carboxylation rate; J: CO_2-saturated electron transport rate; g_m: mesophyll conductance, $R_{photoresp}$: photorespiration, k_c^c: carboxylation efficiency; A_{max}: maximum net assimilation rate; TSP: total soluble protein content; Chl a and b: chlorophyll and b content; Rubisco: Rubisco content; V_i: initial Rubisco activity; V_t: total Rubisco activity; $\Phi(II)$: PSII operating efficiency or quantum yield; F_v/F_m: maximum efficiency of the photosystem II; $\Phi(NPQ)$: non-photochemical quenching; NDVI: normalised difference vegetation index; DPA: Days post anthesis.

INTRODUCTION

Modern agriculture is facing multiple challenges to ensure the food security of a growing population. One of them, and not the least, requires tackling the yield gain stagnation in a context of resource-use sustainability and climate change (FAO, 2017). The release of cultivars tolerant to extreme and highly variable climatic conditions is nowadays required (Korres *et al*., 2016). Studies of genotype *vs* environment to improve breeding efficiency and allow rapid varietal adaptation are crucial to avoid yield vulnerability globally and at the farm level (Atlin *et al*., 2017).

In this context, genomics plays a major role, mainly with the identification of genes related to stress tolerance and yield resilience, to inform genomics-assisted breeding for traits related to crop adaptation to climate change (Scheben *et al*., 2016). However, due to the multigenic and complex nature of yield and responses to the environment, many secondary traits, and consequently underpinning genes, will have differential impacts on adaptation in specific environments (Araus *et al*., 2008; Dwivedi *et al*., 2017). In combination with genomics, advances in phenomics are crucial for unravelling the potential of genotypes to adapt in multiple environments (Zhao *et al*., 2019). Currently, genomics is further advanced compared to phenomics, particularly in terms of the development of high-throughput methods and techniques, creating the so-called phenotype-genotype gap (Furbank & Tester, 2011). While plant phenotyping research has surpassed genomics and proteomics fields in terms of the frequency of publications, more developments are necessary to meet the needs of the research community, breeders, and farmers, especially in developing countries where such facilities are less accessible (Costa et al., 2019; Yang et al., 2020). According to Virlet *et al.* (2022), there is uncertainty as to whether the increasing number of phenotypes measured and the depth of information from the new phenotyping platforms will improve the prediction of quantitative traits. Digital HTP provides a non-destructive and non-invasive method for screening large germplasm panels from plant emergence to maturation. HTP often relies on remote sensing technologies to collect information related to morphological, physiological and phenological traits and provide dynamic information on crop development to understand how the yield is built over time and how it is affected by the environment.

Among the parameters required for screening and subsequently selecting the genotypes for yield stability and stress tolerance, physiological traits are of great importance (Großkinsky *et al*., 2015; Shunmugam *et al*., 2018; Sreeman *et al*., 2018). The physiological breeding approach proposes the selection and crossing of parents with different complex, but complementary traits, to achieve cumulative gene action for yield, while selecting progeny using remote sensing, in combination with genomic selection (Reynolds & Langridge, 2016). This is in accordance with the functional phenomics

concept, a multidisciplinary approach that includes plant physiology, genomics, phenomics, and bioinformatics, aiming to evaluate ideotypes and generate plant models to predict crop behaviour in different scenarios (York, 2019).

The combination of breeding and high-throughput phenotyping (HTP) of physiological traits in plants can have a significant impact, especially in C3 crops such as wheat. According to the yield potential model proposed by Monteith *et al.*, (1977), yield potential is a result of the interaction of the plant with solar radiation through the efficiencies of intercepting and converting light and allocating biomass to the organ of interest, with the conversion efficiency, which is strongly linked to the carbon cycle and photosynthesis, being the variable with highest potential for improvement in C3 plants (Long *et al.*, 2015; Zhu *et al.*, 2010). Current research focuses on finding proxies for physiological and biochemical parameters in plants, mainly with the advent of remote sensing (Jones & Vaughan, 2010) and the requirement for faster screening of multiple genetic materials (Großkinsky et al., 2015), as well as understanding their interaction with the environment (Pauli et al., 2016). Besides mapping phenological changes and yield-components, the use of these proxies for measuring the efficiency of carbon fixation through photosynthesis has assumed a prominent role in crop sciences (van Bezouw *et al.*, 2019). Photosynthesis is generally assessed using gas-exchange instruments, allowing the measurement of the instantaneous variation of CO_2 assimilation and transpiration. CO_2 and light response curves (A-C_i and A-PAR, respectively) provide access to integrative parameters of the functioning of photosynthesis. From those curves, three primary parameters are generally derived: V_{cmax}, J, and A_{max}. Derived from A-C_i curves, V_{cmax} and J are related to the assimilation rate limited by the available CO_2 concentration and by the electron transport required for the regeneration of RuBP, respectively. The A-PAR curve provides information about the point where light is no longer a limiting factor for CO_2 assimilation, often called A_{max} or A_{sat} (Haworth *et al.*, 2018). However, collection of CO_2 and light curve responses as well as net CO_2 assimilation, is time consuming, and often unfeasible at a population scale in field conditions.

Commonly used techniques for indirectly monitoring photosynthesis are based on spectral data enabling computation of spectral reflectance indices or measuring of sun-induced fluorescence (SIF) based on chlorophyll fluorescence measurement by an active sensor (Porcar-Castell *et al.*, 2014; Badgley *et al.*, 2017). In general, spectral indices such as NDVI or its derivatives have been used as an indirect measure of primary production, as they are almost linearly correlated to the fraction of absorbed photosynthetically active radiation (Atzberger 2013). However, it has been shown and it is widely accepted that the photochemical reflectance index (PRI) is the only index able to detect short-term variations of CO_2 assimilation (Dobrowski *et al.*, 2005, Merlier *et al.*, 2015). Recent studies showed the possibility of predicting V_{cmax}, J, and A_{max} combining spectral reflectance and

134 PLSR regression on a small population of wheat in controlled glasshouse conditions and a small set
135 of cultivars in outdoor conditions (Silva-Perez *et al.*, 2018). Meacham-Hensold *et al.* (2019) reported
136 that the predictive aspect of the PSLR works across years, but only on the same genetic materials.
137 The upscaling of those approaches to populations in field conditions is then limited by the need for
138 ground-truth data to build solid and more universal models. The deployment of active sensors for
139 large scale field phenotyping is still complex and so far, few platforms to our knowledge, such as the
140 Field Scanalyzers in the UK and the US, are equipped with chlorophyll fluorescence cameras (Virlet *et*
141 *al.*, 2017; Herritt *et al.*, 2020). Laser induced fluorescence transient (LIFT) is another approach which
142 seems more easily usable on field phenotyping trials, but still requires development for large field
143 trials (Wyber *et al.*, 2018).

144 In this study, we compared remote sensing-based reflectance and fluorescence imaging with
145 traditional approaches to measure and evaluate photosynthesis and fluorescence parameters. At the
146 whole plant scale, NDVI and maximum potential quantum yield were imaged under field conditions
147 (Virlet *et al.*, 2017). Leaf scale fluorescence imaging was realized in controlled environment
148 conditions to collect maximum potential quantum yield, effective quantum yield of PSII, and non-
149 photochemical quenching parameters (Demidchik *et al.*, 2020). Prior to imaging, the same leaves
150 were used for gas exchange and handheld fluorescence measurements, and biochemical analysis
151 were conducted for Rubisco related traits. The biological variability relied on two different wheat
152 cultivars and repeated measurements throughout plant development. Comparison between image
153 variables and traditional approaches was investigated through linear regression models.

154

155 **MATERIAL & METHODS**

156 **Plant material and experimental conditions**

157 The plant material was grown in a controlled environment room at Rothamsted Research,
158 Harpenden, UK, from July to October 2018. The plants were grown under a day length of 16 hours,
159 at temperatures of 18/15°C (day/night), relative humidity of 65/75% (day/night) and irradiance of
160 700 µmols photons m^{-2} s^{-1} (approximately 500 µmols photons m^{-2} s^{-1} at leaf level). Two wheat
161 cultivars (cv. Cadenza and Bobwhite) with contrasting growth and maturation patterns were used.
162 Five wheat seeds were sown in 5 L pots, no thinning was performed, with each pot considered an
163 experimental unit. The experiment was organized into three blocks of five pots of each cultivar, for a
164 total of 30 pots. Zadoks' scale was used for the evaluation of plant development. Plants were
165 phenotyped at the following developmental stages: booting (Z4.5), anthesis (Z6.5) and 7, 14 and 21

166 days after anthesis (Z6.5+7, Z6.5+14 and Z6.5+21, respectively). At each time point, one pot per
167 cultivar and per block was used.

168 **Phenotyping methods**

169 Multiple phenotyping methods were used to evaluate physiological parameters of the plants at
170 whole plant, leaf and biochemical levels. The order of phenotyping was as follows: gas-exchange (A-
171 C_i and A-PAR curves), chlorophyll index, light and dark-adapted chlorophyll a fluorescence through
172 handheld devices and the Phenocenter, fluorescence and reflectance through the Field Scanalyzer,
173 and finally, the biochemical analysis.

174 *Gas-exchange experiments*

175 The response of net photosynthesis (A) to intercellular CO_2 concentration (C_i) and photosynthetic
176 active radiation (PAR) was evaluated through A-C_i and A-PAR curves, performed on the central part
177 of flag leaves, using an infra-red gas analyser model LI6400-XT, with an attached leaf chamber
178 LI6400-40 for combined gas-exchange and fluorescence measurements (LI-COR Biosciences). A-C_i
179 curves conditions were: flow of 200 µmols s^{-1}, block temperature of 20°C, photosynthetic photon
180 flux density (PPFD) of 1800 µmols m^{-2} s^{-1} and relative humidity in the chamber controlled between
181 55 and 65%. The steps of the A-C_i curve were 400, 300, 200, 100, 400, 450, 550, 700, 1000, and 1200
182 µmols mol^{-1} for the reference CO_2 concentration. The A-PAR curves' conditions for flow, block
183 temperature, and relative humidity were the same for A-C_i curves and CO_2 reference concentration
184 was set at 400 µmols mol^{-1}. The steps of the A-PAR curves were 1800, 1400, 1000, 500, 250, 100, 50,
185 and 0 µmols m^{-2} s^{-1} photons.

186 The data from the A-C_i and A-PAR curves were used to calculate additional parameters using the
187 Response Curve Fitting 10.0 and Light Response Curve Fitting 1.0 tools, respectively (available at
188 http://landflux.org/tools). The tool for A-C_i curve is based on the parameter calculation method
189 proposed by Ethier and Livingston (2004) while the A-PAR curve toll uses the method developed by
190 Marshall and Biscoe (1980) and Thornley and Johnson (1990). From the A-C_i curves, the following
191 parameters were modelled/calculated: maximum carboxylation rate (V_{cmax}), CO_2-saturated electron
192 transport rate (J), chloroplastic CO_2 concentration (C_c), inter-cellular CO_2 concentration (C_i),
193 intercellular CO_2 photo-compensation point (C_i*), chloroplastic CO_2 photocompensation point (Γ*),
194 CO_2 compensation point (Γ), CO_2 transfer conductance (g_i), mesophyll conductance (g_m),
195 mitochondrial respiration in the light (R_d), photorespiration ($R_{photoresp}$), carboxylation efficiency (k_c^c).
196 From the A-PAR curves, the following parameters were modelled/calculated: dark respiration (R_{dark}),

197 apparent quantum yield (Φ), light compensation point (LCP) and maximum net assimilation rate
198 (A_{max}).

199 *Fluorescence and SPAD measurements*

200 In addition to the above-mentioned measurements, chlorophyll a content and fluorescence were
201 measured in the same areas of the flag leaves analysed for gas-exchange. The chlorophyll index
202 (SPAD) was measured using the SPAD-502 chlorophyll meter (Konica Minolta). The light-adapted
203 fluorescence parameter, quantum efficiency of PSII ($\Phi(II) = (F_m' - F_s) / F_m'$) was assessed using the
204 following equipment: Fluorpen FP100 (PSI, Φ(II)FP), FMS2 (Hansatech, Φ(II)FM) and Handy Pea
205 (Hansatech, Φ(II)HP). The dark-adapted fluorescence (F_v/F_mHP) was accessed using the Handy Pea
206 after dark adaptation of 30 minutes. Φ(II) was measured with the Fluorpen using the quantum yield,
207 QY function. The saturating light was set up at 3,000 µmols m^{-2} s^{-1} photons. The FMS2 was used in its
208 default setup (Gain = 50, Mod = 3) and measurement was performed over a 2.5 s period, averaging
209 the equivalent F_s signal for 1.8 s before the application of 100-unit saturating pulse over a 0.7 s
210 duration to determine F_m'. The Handy Pea was used in its default configuration. The OJIP curve was
211 measured under light and dark-adapted conditions with only F_v/F_m considered in both conditions.
212 For the light-adapted leaves, the measured F_v/F_m was assumed to be equivalent to Φ(II).

213 *Phenocenter*

214 The same flag leaves that were used for the previous measurements were also used for fluorescence
215 imaging at the Phenocenter (Demidchik *et al*., 2020). The Phenocenter (LemnaTec) is a laboratory-
216 scale, semi-automated system to record and analyse images of plants, through the IMAGING-Pulse-
217 Amplitude-Modulation (PAM) MINI (Waltz). This facility is located in Crop Health and Protection
218 (CHAP), Harpenden, UK. The flag leaves were cut under water using a blade (adapted from Driever *et*
219 *al*., 2014) and then placed in a water reservoir attached to a black surface using double-sided tape.
220 The tips of the flag leaves were also cut to fit the device and inserted into the Phenocenter
221 (Supplementary Fig. S1). Three flag leaves were analysed at a time. For each leaf sample, three
222 circular areas were defined at 25%, 50%, and 75% of the length of the sample. The three values
223 obtained from each area were averaged to calculate the final sample value for all the measured
224 parameters.

225 The leaves were left to adapt to darkness for 30 minutes, inside the Phenocenter. Following this,
226 they were exposed to a saturating light pulse, and F_v/F_m was measured (F_v/F_mPc). This measurement
227 was followed by a light curve, with points at each 20 seconds, at the following PAR levels: 1252,
228 1077, 702, 532, 462, 282, 232, 112, 57, and 2 µmols m^{-2} s^{-1} photons. At these points the efficiency of

229 the photosystem II (Φ(II)) and the non-photochemical quenching (Φ(NPQ)) were measured. An
230 example of the leaf Φ(II) can be seen on Figure 1.

231 *Field Scanalyzer*

232 The pots of the analysed plants were taken to the field and placed on a platform underneath the
233 Field Scanalyzer (LemnaTec) (Supplementary Fig. S2). The Field Scanalyzer is a phenotyping platform
234 (Virlet *et al.*, 2017) installed in a field area at Rothamsted Farm, Harpenden, UK. The CropReporter®
235 (Phenovation) (Jalink & van der Schoor, 2011) chlorophyll fluorescence imager and the Hyperspec®
236 Inspector™ VNIR camera (Headwall Photonic) were used to capture images of the entire plants.

237 The fluorescence was measured at night to collect the F_v/F_m parameter. The camera was positioned
238 at 1m above the top of the plant, and a serie of flashes of red light (620nm) was used to induce the
239 chlorophyll fluorescence (CF) response for 1400 ms (4400 µmols m^{-2} s^{-1} at 70 cm from the bottom of
240 the camera) saturating the electron transfer between the two photosystems (PSII and PSI), and
241 records 24 images within that time. The exposure time of the first image was initiated using the
242 trigger at the rising edge of LED illumination, and this image was called ground fluorescence (F_0). The
243 image with the maximum fluorescence (F_m) was then processed to create a mask to remove the
244 background using the Otsu thresholding approach, which was then applied to the F_0 image. A
245 composite image is then created by combining F_m and F_0 images to obtain the F_v/F_m image to extract
246 the F_v/F_m average values from the plant. Figure 2 shows the final F_v/F_mSc image obtained for
247 Bobwhite and Cadenza at each time point for one of the repetitions.

248 The hyperspectral images were captured on the same day or the following day of the fluorescence
249 measurement, depending on the weather conditions. A white reference panel, Ultra-lightweight
250 Reflectance Target (Zenith Lite™ Ultralight Targets 95%R, Sphereoptics®), mounted on a tripod was
251 also scanned during the acquisition. This panel was used later to convert the raw data into
252 reflectance data using the method describe by Sadeghi-Tehran *et al.* (2021). After segmenting the
253 plant from the background, NDVI was computed from the 680 and 800 nm wavelengths.

254 *Biochemical analysis*

255 The same cut leaves used for the Phenocenter analysis were kept in a tube with water and were
256 transferred to a cabinet to activate photosynthesis and Rubisco for 40 mins before sampling. Cabinet
257 conditions were maintained at 25°C, 70% relative humidity and an irradiance of 900 µmols photons
258 m^{-2} s^{-1} at the leaf level. The samples were taken from the centre of the area using a freeze clamp
259 with 2 cm head diameter, and sample area calculated by measuring the sample width. The samples

260 were immediately transferred to foil packets, snap frozen in liquid nitrogen, and stored at -80°C until
261 analysis.

262 Proteins were extracted from leaf samples as described by Carmo-Silva *et al*. (2017). This protein
263 extract was used to determine Rubisco activity via incorporation of $^{14}CO_2$ in acid-stable products
264 (Carmo-Silva *et al*., 2017), and activation state was calculated from the ratio of initial/total Rubisco
265 activity (V_i, V_t). An aliquot of the homogenate was used to determine chlorophyll a and b content
266 (Chl a and Chl b) using ethanol (Wintermans & de Mots, 1965) and measuring absorbance in a
267 microplate reader SPECTROstar Nano (BMG LabTech). The supernatant prepared for Rubisco activity
268 was also used to quantify total soluble protein (TSP) via the Bradford assay (Bradford, 1976), and the
269 Rubisco content (Rubisco) was determined by [^{14}C] carboxyarabinitol-1,5-bisphosphate (^{14}C-CABP)
270 binding assay (Whitney *et al*., 1999).

271 **Data analysis**

272 In order to conduct gas-exchange, fluorescence and SPAD measurements, as well as Phenocenter
273 and biochemical analysis, two plants of each pot were used as technical replicates, and their values
274 were averaged to form one biological replication for each block. However, for the Scanalyzer
275 analysis, only one value was determined for the whole pot.

276 The data was organized in two factors: two cultivars (cv. Bobwhite and Cadenza) and five
277 developmental stages (Z4.5, Z6.5, Z6.5+7, Z6.5+14 and Z6.5+21), with three blocks, resulting in a
278 total of 30 points. The parameters were split into two groups: image-based parameters obtained
279 from the Field Scanalyzer and the Phenocenter, and the more "traditional" parameters collected by
280 gas-exchange, biochemical analysis and handheld devices.

281 The relationship between the image-based variables and each of the traditional parameters was
282 investigated using linear regression models. The first approach looked at the relationship between
283 the parameters of the two groups (image-based and traditional methods) for each cultivar
284 individually, but with all the development stages (Individual models for Bobwhite and Cadenza). In
285 the second approach, the linear regression was fitted using the whole dataset to analyse the
286 generalist capacity of the regression and analyse the effect of the cultivars. Two models were built
287 for this purpose: one model considered only the regression between the variables of the two groups
288 without the cultivar effect (Generalist model), and the other model considered the cultivar effect
289 (cv.) and its interaction (Int.) with the considered parameter (Interaction model).

290 All the results from the first approach are presented in supplementary data (Supplementary Tables
291 S1 to S4). A subsample is presented in the results section. A subset of five image-based variables

292 were selected and compared to six parameters derived from the CO_2 and light curve response (V_{cmax},
293 J, g_m, k_c^c, $R_{photoresp}$ and A_{max}), to six parameters resulting from the biochemical analysis (TSP, Chl a, Chl
294 b, Rubisco content, V_i and V_t) and five parameters collected by the handheld device (SPAD, Φ(II)FP,
295 Φ(II)FM, Φ(II)HP and F_v/F_mHP). The image-based variables selected were the fluorescence
296 parameters collected with the Field Scanalyzer (F_v/F_mSc), and with the Phenocenter (F_v/F_mPc, $\Phi(II)_{532}$
297 and $\Phi(NPQ)_{1077}$) as well as the NDVI calculated from the reflectance data.

298 ANOVAS were conducted to analyze the results of the regressions for each arrangement. The results
299 of the F-test of the ANOVA (F and *p*-values) and the adjusted coefficient of the determination (R^2_{adj})
300 were used to evaluate the regressions. Tables 1-5 display the F and *p*-values and R^2_{adj} for the
301 Individual Models (Bobwhite then Cadenza), the Generalist Models and the Interactions Models. In
302 Interactions Models, the F and *p*-values of the ANOVA for the parameter in the y-axis are referred to
303 as F (Par.) and *p* (Par.), respectively. The cultivar effect F (cv.) and *p* (cv.) and the interaction effect
304 between cultivars F (Int.) and *p* (Int.) are also noted. For *p* (Par.), a value lower than 0.05 suggests a
305 significant linear correlation between the two analysed parameters. A p-value lower than 0.05 for *p*
306 (cv.) and *p* (Int.) indicates that the intercepts and the slopes of the fitted regression for each cultivar
307 are significantly different. The *p* (Model) and R^2_{adj} are, respectively, the general *p*-value and the R^2_{adj}
308 of the linear regression with the line effect. The cultivar effect tests the hypothesis that the intercept
309 is not different between the two cultivars. A significant effect indicates a statistical difference
310 between the intercept of the two cultivars as well as the two regression lines are mostly parallels.
311 The interaction effect tests the null hypothesis that there is no difference in slopes between the two
312 cultivars, which indicates that both cultivars are responding similarly.

313 The residuals of the linear regressions were evaluated for normality, homoscedasticity (homogeneity
314 of variances) and independence by visually checking the Q-Q, residuals *vs* fitted values and
315 histogram of residuals' plots, and also by the Shapiro-Wilk test. The most relevant linear regressions
316 were plotted (Supplementary Fig. S3-S7) and the results were presented in tables 1 to 5. The R
317 software was used for the analyses with the following packages *ggpmisc*, *stats* and *olsrr* (R Core
318 Team, 2020).

319

320

321 **RESULTS**

322 **Date and cultivar effect**

Among the presented variables, two main patterns were observed (Fig. S3, Supplementary Table S5). The first showed a significant decrease of the values for both cultivars from booting (Z4.5) to 21 days post anthesis (Z6.5+21) for all the variables derived from the gas-exchange (V_{cmax}, J, g_m, k_c^c, $R_{photoresp}$ and A_{max}), for the biochemical parameters related to the Rubisco (TSP, Rubisco, V_i and V_t) as well as for Φ(II)HP and F_v/F_mHP. The same was observed for the image variable $\Phi(NPQ)_{1077}$. The second pattern showed a contrasted behaviour between the two cultivars for Φ(II)FM and the image variables F_v/F_mSc, F_v/F_mPc, and NDVI with a significant decrease overtime for Cadenza, whilst no significance differences were observed for Bobwhite.

The chlorophyll related parameters (Chl a, Chl b and SPAD) showed an increase of the values peaking at Z6.5+7, followed by a decrease for Cadenza and no significant variation for Bobwhite. For $\Phi(II)_{532}$, the values decreased significantly Z6.5+14 for Cadenza, whilst for Bobwhite the values dropped significantly after booting with no more variation for the rest of the experiment. Finally, Φ(II)FP did not show significant variation for either cultivar with, however, a decreasing trend observed for Cadenza at Z6.5+14 and Z6.5+21.

Field Scanalyzer

Dark-adapted chlorophyll fluorescence (F_v/F_mSc)

The F_v/F_mSc calculated from images of the Field Scanalyzer for whole plants (Fig. 2) showed high correlations with most of the parameters measured by traditional methods (Table 1; Supplementary Fig. S3). Cadenza showed significant correlations with all the parameters, with the highest fitting for V_i (R^2_{adj} = 0.75) and the lowest fitting for k_c^c and Chl b (R^2_{adj} = 0.33). For Bobwhite, the regressions between F_v/F_mSc and (i) the gas-exchange parameters were all significant (R^2_{adj} = 0.32 – 0.61), (ii) the biochemical parameters were mostly all significant (R^2_{adj} = 0.24 – 0.62) except for the Chl a and b content and (iii) the handheld devices were significant only for Φ(II)FP (R^2_{adj} = 0.29) and F_v/F_mHP (R^2_{adj} = 0.43).

The choice of the cultivar appeared to impact the relationship between the traditional parameters and the imaging F_v/F_mSc (Fig. 3). The Interaction Models (Table 1) confirmed that most of the parameters displayed a significant cultivar (cv.) effect except for the parameters k_c^c, $R_{photoresp}$, A_{max}, Φ(II)FP, Φ(II)HP, F_v/F_mHP. When the cv. effect was significant, the R^2_{adj} from the Interaction Model increased compared to the Generalist Model. On the other hand, the R^2_{adj} between both models were quite similar when no significant cv. effect was observed. No significant interaction between the parameters and cultivar effect was observed, except for Chl a and b, indicating that in most

354 cases, there is no significant difference between the slopes of the regression of the parameters and
355 F_v/F_mSc of each cultivar.

356 *Normalized Difference Vegetation Index (NDVI)*

357 The regressions analysis between the NDVI measured by the Field Scanalyzer and other parameters
358 displayed a completely different pattern to the previous observation with F_v/F_mSc. All the linear
359 regressions were significant for Cadenza, whereas no significant regressions were observed for
360 Bobwhite (Table 2; Supplementary Fig. S4). Cadenza showed high correlations for most of the
361 parameters, regardless of the type of measurement with R^2_{adj} ranging from 0.55 to 0.84 for the gas-
362 exchange parameters, 0.31 to 0.79 for the biochemical parameters, and 0.42 to 0.75 for handheld
363 devices. The Generalist Models were clearly impacted by the lack of responsiveness of the ground
364 variables to changes in NDVI for Bobwhite, displaying lower but still significant R^2_{adj} for most
365 parameters (R^2_{adj} = 0.16 – 0.53), except for Chl b and SPAD. However, the Interaction Models did not
366 show a clear cultivar effect for all the parameters. Significant cv. effects were only observed for V_{cmax}
367 among the gas-exchange parameters, for Chl a and Chl b for the biochemical parameters and for
368 SPAD, Φ(II)FP and F_v/F_mHP. Incorporating the cv. effect into the Interaction Model improved the
369 regressions in most cases (R^2_{adj} = 0.29 – 0.60), except for g_m. Significant interactions were found for
370 Chl a, b SPAD and Φ(II)FM, confirming the different behaviour of Bobwhite in its responses to NDVI
371 (Fig. 3).

372 **Phenocenter**

373 *Dark-adapted chlorophyll fluorescence (F_v/F_mPc)*

374 The F_v/F_mPc calculated through the IMAGING-PAM at the Phenocenter for the flag leaves (Fig. 1) also
375 showed that the linear regressions were strongly affected by the cultivar (Table 3; Supplementary
376 Fig. S5). Cadenza demonstrated high and significant correlations with all the parameters measured
377 by gas exchange (R^2_{adj} = 0.57 – 0.85), biochemical analysis (R^2_{adj} = 0.35 – 0.76) or handheld device
378 (R^2_{adj} = 0.50 – 0.82), with the highest fits observed for J, Φ(II)FM and F_v/F_mHP (R^2_{adj} = 0.85, 0.81 and
379 0.82, respectively) and the lowest fits for Chl a and b (R^2_{adj} = 0.44 and 0.35, respectively). For
380 Bobwhite, significant regressions were only observed between F_v/F_mPc and the parameters from the
381 biochemical analysis, Chl a and Chl b and the parameters from the handheld devices, Φ(II)HP (R^2_{adj} =
382 0.32, 0.25 and 0.45, respectively). All the regression showed a significant R^2_{adj} for the Generalist
383 Models. Since most of the regressions for Bobwhite were non-significant, it was expected that a
384 cultivar effect would be present for most parameters.However, the Interaction Models only showed
385 a significant cv. effect for A_{max}, SPAD, Φ(II)FP, Φ(II)HP and F_v/F_mHP. This indicates that for these five

386 parameters, the offset of the regression differs significantly between cultivars. The only significant
387 interaction was found for Φ(II)HP, indicating that in this case, the slopes were significantly different
388 between cultivars only for Φ(II)HP. In general, the R^2_{adj} between the Generalist and the Interaction
389 Models were similar, with the exception of the five parameters that had a significant cv. effect. For
390 those, improvements to the regressions were achieved by considering the cv. effect into the
391 Interaction Models.

392 *Photosystem II quantum efficiency ($\Phi(II)_{532}$)*

393 The $\Phi(II)_{532}$ was calculated through the Phenocenter IMAGING-PAM, at 532 µmols m^{-2} s^{-1} photons
394 during a light curve at flag leaf level (Fig. 1). The regressions between $\Phi(II)_{532}$ and most of the
395 parameters displayed a significant cultivar effect except for Chl a, b and SPAD (Table 4,
396 Supplementary Fig. S6). Cadenza presented significant correlations with all the parameters
397 measured either by gas-exchange (R^2_{adj} = 0.59 – 0.84), biochemical analysis (R^2_{adj} = 0.32 – 0.83) or
398 handheld device (R^2_{adj} = 0.31 – 0.90), with the highest fittings for J, A_{max}, TSP, V_t and F_v/F_mHP (R^2_{adj} =
399 0.82, 0.84, 0.82, 0.83 and 0.90, respectively) and the lowest fittings for Chl b and Φ(II)FM (R^2_{adj} =
400 0.32 and 0.31, respectively). For Bobwhite, the regressions between $\Phi(II)_{532}$ and the gas-exchange
401 parameters were all significant (R^2_{adj} = 0.36 – 0.63), whereas the regression with the biochemical
402 parameters and the handheld devices parameters were only significant for TSP, V_i, V_t, Φ(II)FP and
403 F_v/F_mHP (R^2_{adj} = 0.37, 0.27, 0.31, 0.28 and 0.34, respectively). As already indicated, most of the
404 parameters (except for Chl a, b, and SPAD) showed a significant cv. effect, indicating that the
405 intercept of linear regressions for each of the cultivars was significantly different. Among those
406 parameters V_{cmax}, g_m, k_c^c, $R_{photoresp}$, TSP, Rubisco, V_i, Φ(II)FP and Φ(II)HP did not show significant
407 interactions, indicating that the slopes of the linear regression for each cultivar were not significantly
408 different. The relationship between $\Phi(II)_{532}$ and those nine parameters followed a similar pattern,
409 with only intercepts differing between cultivar. As expected, the Generalist Models were affected by
410 the cultivar. The R^2_{adj} was not significant for A_{max}, Φ(II)FP, Φ(II)HP and F_v/F_mHP, and was low to
411 moderate, but significant, for the other parameters (R^2_{adj} = 0.14 – 0.44). Considering the cultivar
412 effect in the Interaction Model substantially improved the models for all the parameters, with R^2_{adj}
413 ranging from 0.32 to 0.77.

414 *Non-photochemical quenching ($\Phi(NPQ)_{1077}$)*

415 The $\Phi(NPQ)_{1077}$, calculated using the Phenocenter IMAGING-PAM, at 1077 µmols m^{-2} s^{-1} photons
416 during a light curve at flag leaf level was showing significant linear regressions for most of the
417 parameters and for both cultivars (Table 5; Supplementary Fig. S7). However, in this case, Cadenza
418 presented significant correlations for only a few parameters measured (i) by gas exchange: V_{cmax}, J,

419 $R_{photoresp}$ and A_{max} (R^2_{adj} = 0.24 – 0.49), (ii) by biochemical analysis: TSP, Rubisco, V_i and V_t (R^2_{adj} = 0.35
420 – 0.46), and by handheld device: SPAD, Φ(II)FM, Φ(II)HP and F_v/F_mHP (R^2_{adj} = 0.28 – 0.54) with the
421 best fits for J, A_{max}, TSP, SPAD and F_v/F_mHP (R^2_{adj} = 0.49, 0.47, 0.46, 0.47 and 0.54, respectively). For
422 Bobwhite, the regressions with (i) the gas-exchange parameters were all significant (R^2_{adj} = 0.78 -
423 0.89), (ii) the biochemical parameters were mostly significant (R^2_{adj} = 0.36 – 0.76), except for the Chl
424 a and b content, and (iii) the handheld devices were significant only for Φ(II)FP, Φ(II)FM and F_v/F_mHP
425 (R^2_{adj} = 0.25, 0.21 and 0.65, respectively). It should be noted that for $Φ(NPQ)_{1077}$, the R^2_{adj} were
426 higher for Bobwhite for the gas-exchange and biochemical parameters, as well as for F_v/F_mHP of the
427 handheld devices. The Generalist Models showed signification R^2_{adj} for most of the parameters (R^2_{adj}
428 = 0.23 – 0.63), except for Chl a, b and SPAD. The Interaction Models showed significant cv. effects for
429 V_{cmax}, J, TSP, Chl a and b, V_t, SPAD and Φ(II)FM, indicating a significantly difference between the two
430 cultivars. However, for these parameters, except for SPAD, the interactions were not significant,
431 indicating a similar slope for the regressions for both cultivars. Nonetheless, including the cv. effect
432 in the Interaction Models improved the R^2_{adj} for the aforementioned parameters compared to the
433 Generalist Models, whilst having little effect on the R^2_{adj} for the other parameters compared to the
434 Generalist Models.

435

436 **DISCUSSION**

437 *Model performances and cultivar effect*

438 The present study aimed to model photosynthetic parameters collected at leaf scale through gas-
439 exchange and by biochemical analysis using imaging technology. Five image variables collected at
440 pot scale in the field (NDVI and F_v/F_mSc) and at leaf scale in laboratory conditions (F_v/F_mPc, $Φ(II)_{532}$
441 and $Φ(NPQ)_{1077}$) were investigated as potential targets for further screening of photosynthetic
442 parameters in phenotyping trials. Overall, the results showed the possibilities to build linear models
443 to predict photosynthesis parameters based on the image variables, despite the varying
444 performance of the two cultivars. The Interaction Models proved that considering the cultivar effect
445 improved the models R^2_{adj} when the cultivar effect was significant compared to the Generalist
446 Models. The linear regression model performances were largely driven by the phenotypic variability
447 resulting from the stage of development of the two cultivars. As senescence progressed, a decrease
448 of the phenotypic values for each cultivar was observed for all the gas exchange parameters (V_{cmax}, J,
449 g_m, k_c^c, $R_{photoresp}$ and A_{max}) as well as the Rubisco related parameters (TSP, Rubisco, V_i, V_t), the
450 fluorescence parameters F_v/F_mHP collected with the HandiPEA and $Φ(NPQ)_{1077}$ measured at the
451 Phenocenter. A contrasting behaviour was observed between Bobwhite and Cadenza for chlorophyll

452 variables (Chl a and b, SPAD) and the Φ(II) parameters measured by the handheld devices. The same
453 was observed for the other four image variables. Cadenza followed the same senescence pattern
454 with a decrease in phenotypic values with the senescence, explaining the good agreement between
455 the image and the ground variables. The lower model performances with $\Phi(NPQ)_{1077}$ were due to
456 the fact that a significant decrease of NPQ could only be seen at 21 days post anthesis (DPA). The
457 low model performances between the five image variables and the chlorophyll index resulted from
458 the fact that the chlorophyll amount increased up to 7 DPA before decreasing. In contrast, Bobwhite
459 displayed a different pattern with no significant variation of the phenotypic values across the five
460 dates of measurement for the chlorophyll variables (Chl a and b, SPAD), the Φ(II) variables as well as
461 for F_v/F_mSc, NDVI, F_v/F_mPc. While no significant decreases were observed for F_v/F_mSc, a decreasing
462 trend was still observed, which explains why the model performances were similar to Cadenza. A
463 decreasing trend was also observed for NDVI without significant differences between dates.
464 However, the small day-to-day fluctuations explained the absence of correlation with the
465 photosynthetic variables. The absence of trend and significant differences between dates of F_v/F_mPc
466 explained the absence of correlations with the ground variables for Bobwhite. The relatively good
467 performance of Bobwhite for $\Phi(II)_{532}$ seems to be due to the first date having a significant higher
468 value than the four other dates.

469 The observed patterns in Cadenza correspond to a typical wheat senescence pattern with a gradual
470 decrease in photosynthetic capacity along with the degradation of the chlorophyll (Thomas &
471 Howarth, 2000). On the other hand, Bobwhite is known as a slow maturaturing cultivar (Mackintosh
472 *et al.*, 2006), and it was expected to see delayed decrease in phenotypic values for both
473 photosynthesis and chlorophyll variables, or a slower maturation compared to Cadenza, which
474 would correspond to a Type A or B stay green phenotype according to Thomas & Howarth (2000).
475 However, the current results suggest Bobwhite may belong to Type C (also called cosmetic stay-
476 green) which is described as undergoing a degradation of the photosynthetic activity as normal with,
477 however, no sign of degradation of the chlorophyll, which corresponds to the results observed in this
478 study, at least up to the end of the experiment at 21 days after anthesis. According to Thomas and
479 Ougham (2014), breeders tend to avoid using cosmetic stay-greens because they do not offer any
480 yield benefits. The opposite type, functional stay-green, is more desirable for breeding purposes as
481 photosynthesis is maintained longer during the maturation phase (Thomas & Ougham, 2014; Li *et*
482 *al.*, 2022). However, screening populations for functional stray-green genotypes is complicated as it
483 would require gas-exchange measurements at multiple time points on a large number of individuals,
484 which is not feasible without a large number of instruments and trained users. Currently,
485 phenotyping studies on stay-green genotypes are based on screening materials with visual scoring,

486 SPAD, RGB images or spectral indices, without being able to distinguish cosmetic from functional
487 genotypes (Pinto *et al.*, 2016; Christopher *et al.*, 2018, Hassan *et al.*, 2021, Chapman *et al.*, 2021).
488 The last five years have seen successful studies predicting V_{cmax} and J using spectral data (Silva-Perez
489 *et al.*, 2018; Meacham-Hensold *et al.*, 2019, Montes *et al.*, 2022). It would be interesting to see if
490 those approaches can overcome the challenges of identifying functional stay green phenotype in
491 field conditions.

492 *Image variables vs traditional approaches*

493 The results showed the image variables, tested at the plant scale (NDVI and F_v/F_mSc), and at the leaf
494 scale (F_v/F_mPc, $\Phi(II)_{532}$ and $\Phi(NPQ)_{1077}$) constitute good to strong estimators of the gas-exchange
495 (V_{cmax}, J, g_m, k_c^c, $R_{photoresp}$ and A_{max}) and the biochemical variables (TSP, Rubisco, V_i and V_t), when
496 senescence is driving the variability. As mentioned above, the model performances have been
497 strongly influenced by the cultivar disparity in term of the senescence patterns, resulting in strong
498 specificity between the ground variables and their relationship with the image-based variables. The
499 highest predictions for the gas-exchange variables were obtained with $\Phi(NPQ)_{1077}$ (R^2_{adj} = 0.78-0.89)
500 for the cultivar Bobwhite. NDVI, F_v/F_mPc and $\Phi(II)_{532}$ were also strong estimators for V_{cmax}, J and A_{max}
501 with the cultivar Cadenza. Lower performances were obtained using F_v/F_mSc but with acceptable
502 results (R^2_{adj} ~ 0.50). However, it was not possible to conclude which of the image variables was the
503 most relevant to investigate a particular parameter in the photosynthetic measurements collected
504 by gas-exchange or biochemical analysis.

505 NDVI has been used extensively over decades to monitor vegetation dynamics and quantify green
506 biomass at various scales (landscape to plot). It is well accepted that NDVI is not the most suitable
507 index to monitor instantaneous change in net CO_2 assimilation (Gamon *et al.*, 1995, Dobrowski *et al.*,
508 2005; Urban *et al.*, 2013). However, a few studies showed significant relationship between NDVI and
509 net CO_2 assimilation, mostly driven by the genetic variability as well as by the stages of development,
510 similarly to our study (Kumari *et al.*, 2012; Gonzalez-Dugo *et al.*, 2015; Camino *et al.*, 2018). Studies
511 in the literature looking at the link between NDVI and gas-exchange and biochemical parameters are
512 scarce to our knowledge. Letts *et al.* (2008) found an absence of correlation between A_{max} and NDVI
513 while Zhou *et al.* (2014) showed a high correlation with V_{cmax} on deciduous forest trees, mainly due
514 to the different phenological stages. Despite the absence of correlation observed for Bobwhite, due
515 to the reasons discussed, the Interaction Models showed that it was possible to use NDVI to predict
516 the different parameters related to carbon assimilation, either derived from A-C_i and A-Par curve
517 (V_{cmax}, J, g_m, k_c^c, $R_{photoresp}$, A_{max}) or from biochemical analysis (V_i and V_t) but not the Rubisco activation
518 state (Act, Table S3). The same was observed for N related parameters (TSP and Rubisco) and

519 chlorophyll pigment (Chl a and b, SPAD). Despite the strong discrepancy existing between the two
520 cultivars caused by their senescence behaviour, the Interaction Models showed that NDVI could be a
521 predictor for those variables with acceptable results. Gitelson *et al.* (1998, 2003) showed that NDVI
522 was far from the best index to predict chlorophyll content at leaf scale due to its lack of sensitivity
523 from medium chlorophyll concentration. However, other studies proved that, at the canopy scale,
524 NDVI might be a useful indicator if no other indices are available (Zarco-Tejada *et al.*, 2005; Camino
525 *et al.*, 2018; Alordzinu *et al.*, 2021).

526 The maximum efficiency of the photosystem II (F_v/F_m) is commonly used as an indicator of plant
527 health status and to monitor stress responses in large population screening, as it is extremely
528 difficult to screen population for gas-exchange, especially in field conditions (Pask *et al.*, 2012).
529 However, Pask *et al.* (2012) noted that F_v/F_m may not always be a reliable indicator of crop
530 performance. While F_v/F_m is often used as a proxy for photosynthetic performance in phenotyping,
531 its link with gas exchange measurements is not yet fully established. Some studies have found
532 positive correlations with mixed success for V_{cmax} (R^2 = 0.02 - 0.13 and R^2 = 0.11 to 0.47 in Zhuang *et*
533 *al.*, 2020 and Mission *et al.*, 2006, respectively), J (R^2 = 0.09 – 0.28 in Zhuang *et al.*, 2020) and A_{max} (R^2
534 = 0.52, Ishida *et al.*, 2014). In the present study, the cultivar models performance for gas-exchange
535 (V_{cmax}, J, g_m, k_c^c, $R_{photoresp}$, A_{max}) and biochemical parameters (V_i, V_t) with F_vF_mPc ranged from 0.57 to
536 0.85 for Cadenza and are nearly zero for Bobwhite due to its senescence behaviour. The same would
537 have been expected at the whole plant scale (F_v/F_mSc). However, the R^2_{adj} range of the two cultivars
538 was between 0.32 to 0.75. Whilst results showed no significant differences between dates, a
539 decreasing trend was observed, leading to an increase in model performances for Bobwhite at the
540 whole plant scale. Despite the contrasting results between the two sets of measurements, the
541 Interaction models gave similar performances, ranging from 0.28 to 0.66. This suggests that F_v/F_m is
542 a reliable indicator of photosynthetic performance at a seasonal scale, regardless of the
543 measurement environment. Using F_v/F_m as a predictor of the chlorophyll content (Chl a, b and SPAD)
544 or the protein content variables (TSP, Rubisco) gave low to high performances depending on the
545 cultivar (*i.e.*, senescence behaviour) and the scale of the measurement. These findings are consistent
546 with the previous literature, which has reported high correlations between Fv/Fm and these
547 variables accross different stages of development (Peng *et al.*, 2017, Hailemichael *et al.*, 2016, Jia *et*
548 *al.*, 2019) and/or under various nitrogen or irrigation treatments (Jia *et al.*, 2019, Zarco-Tejada *et al.*,
549 2013).

550 The PSII operating efficiency (Φ(II)), also known as quantum efficiency, provides an overall
551 measurement of the efficiency of the PSII reaction centre in light conditions (Genty *et al.*, 1989). This
552 parameter indicates the proportion of light absorbed by chlorophyll associated with PSII that is used

553 in photochemistry, and is strongly correlated with net CO2 assimilation (McAusland *et al.*, 2013). It is
554 also affected by the degradation of the photosystem during senescence as demonstrared in Mu *et*
555 *al.* (2010) and Dai *et al.* (2004) where Φ(II) began to decrease significantly after 15 DPA. Similarly,
556 Kong *et al.* (2015) observed a significant decrease in Φ(II) around the same time period. In the
557 present study significant differences in $\Phi(II)_{532}$, Φ(II)FM and Φ(II)HP for Cadenza were observed after
558 14 DPA, consistent with previous research (Fig. 3). However, variations between dates were not
559 uniform across instruments. No significant difference was observed between dates for Cadenza and
560 Bobwhite with Φ(II)FP, as well as Φ(II)FM for Bobwhite. For Φ(II)HP, values reached their peak at 7
561 DPA and were significantly different at 28 DPA, while for $\Phi(II)_{532}$, the highest values were at booting
562 and no significant differences were observed from anthesis to 28 DPA. The present study showed
563 that Φ(II) under moderate light is a good estimator for carbon assimilation related parameters
564 measured either by gas-exchange (V_{cmax}, J, g_m, k_c^c, $R_{photoresp}$, A_{max}) or derived from biochemical
565 analysis (V_l and V_t). Except for k_c^c, the model performances were better for Cadenza than for
566 Bobwhite, possibly due to the absence of significant differences between dates mentioned above.
567 High and positive correlations between Φ(II) and V_{cmax}, J, A_{sat} and g_m were also found in Sun *et al.*
568 (2014), with variation caused by contrasted levels of ozone. Almaida *et al.* (2021) also observed
569 positive correlations with A_{max} and V_{cmax} resulting from genetic variability of the sugar cane cultivars
570 and wild types. Using Φ(II) as a predictor of the chlorophyll content will give reasonable results as
571 long as both variables behave similarly during senescence.

572 Non-photochemical quenching (NPQ) is one of the three main mechanisms for dissipating the energy
573 of the light absorbed by the chlorophyll pigments. NPQ competed with the photochemistry and the
574 re-emission of the energy as a photon of fluorescence (Porcar-Castell *et al.*, 2014). NPQ is a
575 photoprotective mechanism removing the excess excitation energy within the chlorophyll-containing
576 complexes (Murchie and Lawson, 2013). However, contradictory results have been reported in the
577 literature regarding changes of NPQ after anthesis and during the senescence in wheat. Some
578 authors observed an increase of NPQ during the period post anthesis period, with measurements
579 performed either in the morning or at midday (Dai *et al.*, 2004), and in different shading conditions
580 (Mu *et al.*, 2010). Xu *et al.* (2017) and Shao *et al.* (2013) observed an increase in NPQ peaking at 21
581 and 30 DPA, respectively, before decreasing. However, Kong *et al.* (2015) reported a significant
582 decrease of NPQ measured on the flag leaves from anthesis to 32 DPA, and Peng *et al.* (2021)
583 observed a decrease in NPQ between anthesis and maturity stages in wheat grown with various
584 nitrogen inputs. The results of the present study showed a decreasing trend in $\Phi(NPQ)_{1077}$ from
585 anthesis, becoming significant from 21 DPA for both cultivars compared to anthesis time. The
586 model's performances with the photosynthesis parameters derived from gas-exchange and from

587 biochemical analysis were higher for Bobwhite (R^2_{adj} = 0.78 - 0.89) than Cadenza, indicating a better
588 match between the senescence pattern of $\Phi(NPQ)_{1077}$ and those variables in Bobwhite. Negative
589 correlations with net CO_2 assimilation have been reported (Ishida *et al.*, 2014, Zarco-Tejada *et al.*,
590 2013), but no data concerning A_{max} or the other parameters derived from the A-C_i and A-PAR curves
591 could be found in the literature to our knowledge. Negative correlations with Chl a content have
592 been also reported in Ishida *et al.* (2014) and Zarco-Tejada *et al.* (2013), mainly driven by drought.

593 The handheld fluorescence devices were used as comparison with the fluorescence imagers, as well
594 as with NDVI. While the use of NDVI to estimate F_v/F_m and Φ(II) could be questionable, the results
595 did not differ much from those reported in the literature, and low to moderate relationships were
596 observed (Peng *et al.*, 2017; Tan *et al.*, 2012, Jia *et al.*, 2019). The difference in performance
597 between Bobwhite and Cadenza is attributed to their senescence behaviour, as discussed earlier.
598 Usually, indices such as PRI, red-edge indices and fluorescence band indices are preferred to report
599 variation in fluorescence. However, the hyperspectral image collection was done under non-optimal
600 outdoor conditions, with variable ambient illumination between the end of September and the
601 beginning of November in the UK. Consequently, the above-mentioned indices would not be reliable
602 to report the variations in fluorescence, as the conditions between acquisition dates were too
603 inconsistent.

604 The variation of F_v/F_m measured by the two imagers reflected the variation of F_v/F_m measured using
605 the HandyPea for Cadenza. For Bobwhite, although no significance difference was observed between
606 date for F_v/F_mSc at the plant scale, the observed decreasing trend explained the relatively good
607 correlation with the value collected with HandyPea. The measurements resulting from the
608 Phenocenter did not show variations between time points, while the data collected with the
609 HandyPea on the same leaves showed a significant decrease over time. The results are unexpected
610 as the leaves were cut from the plants just before being imaged by the fluorescence of the
611 Phenocenter, and no sensible explanation could be found.

612 The variation of $\Phi(NPQ)_{1077}$ was better reflected by the variation of F_v/F_m than by Φ(II), in agreement
613 with Kong et al (2015), where the decrease in NPQ appeared to be more concomitant with the
614 decrease of F_v/F_m than with the decrease of Φ(II). The authors also mentioned a regional accordance
615 of imaging F_v/F_m and NPQ across the leaves, concluding that this would indicate that NPQ is closely
616 associated with the quantum efficiency of PSII photochemistry.

617 *Throughput consideration of the different approaches*

618 Reynolds *et al.* (2012) noted that breeders are interested in reducing the size of their test
619 populations to achieve the desired genotype at a reasonable probability and cost, even if the
620 methods may be imperfect from a physiological and theoretical standpoint. In the case of
621 photosynthetic traits, gas-exchange and biochemical analysis represent the gold standards but are
622 also considered low throughput. The time required to perform an A-C_i followed by an A-PAR curve
623 takes approximately 50-60 minutes per flag leaf for an experienced user in controlled conditions.
624 Biochemical analysis involves destructive sampling that also requires processing (freeze drying,
625 grinding, etc) before quantification of TSP, Rubisco and enzymatic reactions. Handheld fluorescence
626 instruments are used for pre-screening of populations for photosynthesis performance using either
627 Φ(II) or F_v/F_m as they are quite fast. Measuring Φ(II) with the Fluorpen is straightforward and takes
628 only 10 seconds per leaf, potentially allowing for measurement of 360 leaves per hour, which is the
629 fastest instrument to our knowledge. However, as shown in this study, the correlations with image
630 fluorescence are weaker than those obtained with the HandyPea and the FMS2.

631 The advantages of HTP methods are the higher phenotyping capacity and, in some cases, the
632 reduced necessity of human intervention. However, the throughput is highly dependent of the type
633 of the technologies used. For example, in the case of the Phenocenter, an operator is required to
634 program the execution, but the measurements are automatic and there is the possibility to perform
635 an automatic loading of sample, pre inserted in the machine. The time frame for measuring F_v/F_m,
636 followed by a light curve for Φ(II) and Φ(NPQ), on three flag leaves is around 40 minutes, including
637 the 30 minutes of dark adaptation. The system should be able to host several boxes of three leaves
638 for dark adaptation, allowing to measure 18 leaves per hour in total. The Field Scanalyzer requires an
639 operator to program the platform, but the platform runs automatically over the full experiment once
640 it is launched. The throughput of the fluorescence camera is 40 plots (or pots) per hour, but this
641 includes the time it takes to move the camera between targets. The visible diameter of the flash
642 used to induce fluorescence is 1.2 to 1.4 meters, which can also trigger a response to light in nearby
643 plots. Therefore, the device must be carefully routed to measure each plot in complete dark
644 adaptation, which decreases the camera's throughput. The hyperspectral camera, set up in medium
645 spatial resolution (Sadeghi-Tehran *et al.*, 2021), allows collection of 26 scans per hours. As the area
646 covered is about 1.8 x 1.5 m, the number of plots or pots scanned will vary depending on the size of
647 targets. The two phenotyping platforms discussed in the previous paragraph offer significant
648 advantages over gas-exchange measurements in terms of speed and reduced human intervention.
649 However, their throughput is still quite low compared to handheld fluorescence instruments, which
650 are commonly used as proxy of photosynthesis. Nonetheless, spectral data are still promising for
651 fluorescence and photosynthetic traits. The Fraunhofer Line Depth (FLD) can be used to retrieve sun-

652 induced fluorescence (Porcar-Castell *et al.*, 2014) and the last decade have seen an increase of
653 prediction of V_{cmax} and J using the full range of spectral data (Silva-Perez *et al.*, 2018; Meacham-
654 Hensold *et al.*, 2019, Montes *et al.*, 2022). Most of those developments have relied on single
655 spectroradiometer, as they are much faster than the imager mounted on ground-based system.
656 However, hyperspectral imaging with UAV provides data on large scale, enabling access to those
657 traits at lower spatial resolution (Zarco-Tejada *et al.*, 2013; Camino *et al.*, 2018, 2019).

658 *Conclusion*

659 The present study showed that photosynthetic traits obtained either by gas-echange or biochemical
660 analysis could be monitored and quantified susccesfully using imaging technologies as long as the
661 senescence is driving the variability. Despite the contrasted behaviour between the two cultivars,
662 Bobwhite and Cadenza, linear regression models which account for both the cultivar and the
663 interaction effects, further improved the modelling of photosynthesis indicators. Future work will be
664 necessary to evaluate the link between the image variables and gas-exchange during earlier stages
665 of development. The results also showed the importance of prior knowledge of the stay green type
666 of the cultivar used, as it can strongly impact the outcomes. It also emphasises the need to develop
667 sensitive enough approaches to differentiate cosmetic from functional stay green genotypes that
668 breeders can use for photosynthetic traits.

669 **Supplementary data**

670 Th following supplementary data are available at the JXB online:

671 Fig. S1. Flag leaf holder for Phenocenter analysis

672 Fig. S2. Pots settings under the Field Scanalyzer

673 Fig. S3. Linear regressions between Fv/FmSc and selected variables

674 Fig. S4. Linear regressions between NDVI and selected variables

675 Fig. S5. Linear regressions between F_v/F_mPc and selected variables

676 Fig. S6. Linear regressions between $\Phi(II)_{532}$ and selected variables

677 Fig. S7. Linear regressions between $\Phi(NPQ)_{1077}$ and selected variables

678 Table S1. Linear regressions parameters between images and A-C_i curves

679 Table S2. Linear regressions parameters between images and A-PAR curves

680 Table S3. Linear regressions parameters between images and biochemical variables

Table S4. Linear regressions parameters between images and handhled devices variables

Table S5. Mean and standard deviation for each variables per date and per cultivar

Dataset S1: Phenotypic data

Acknowledgments

We thank Kirsty Hassal and Jess Evans for their help in disigning the experiment and their advice in the analysis of the data (Rothamsted Research), Fiona Gilzean for the access to the CE room and cabinet for growth of the plants.

Author contributions

JPP and NV designed and performed the experiments and analysed data; TA performed the image acquisition at the PhenoCenter (CHAP), PST performed the image extraction and analysis from the Field Scanalyzer; DO and ECS peformed the biochemical analyses; NV and JPP wrote the manuscript; NV, JPP, TA, PST, DO, ECS and MJH revised and edited the manuscript; JPP, ECS and MJH enabled to secure funding for the project leading to this publication. All authors reviewed and approved the final manuscript.

Conflict of interest

The authors declare no conflict of interest.

Funding

Rothamsted Research receives grant-aided support from the Biotechnology and Biological Sciences Research Council (BBSRC) of the Delivering Sustainable Wheat strategic program (BB/X011003/1).

Data availability

All data supporting the findings of this study are available within the paper and within its supplementary data published online.

REFERENCES

Almeida RL, Silveira NM, Pacheco VS, Xavier MA, Ribeiro RV, Machado EC. 2021. Variability and heritability of photosynthetic traits in Saccharum complex. Theoretical and Experimental Plant Physiology **33**, 343-355.

Alordzinu KE, Li J, Lan Y, Appiah SA, Al Aasmi A, Wang H, Liao J, Sam-Amoah LK, Qiao S. 2021. Ground-based hyperspectral remote sensing for estimating water stress in tomato growth in sandy loam and silty loam soils. Sensors (Basel) **21**, 5705.

Araus JL, Slafer GA, Royo C, Serret MD. 2008. Breeding for yield potential and stress adaptation in cereals. Critical Reviews in Plant Sciences **27**, 377-412.

Atlin GN, Cairns JE, Das B. 2017. Rapid breeding and varietal replacement are critical to adaptation of cropping systems in the developing world to climate change. Global Food Security **12**, 31-37.

Atzberger C. 2013. Advances in remote sensing of agriculture: context description, existing operational monitoring systems and major information needs. Remote Sensing **5**, 949-981.

Badgley G, Field CB, Berry JA. 2017. Canopy near-infrared reflectance and terrestrial photosynthesis. Science Advances **3**, e1602244 doi: 10.1126/sciadv.1602244

Bradford MM. 1976. A rapid and sensitive method for the quantitation of microgram quantities of protein utilizing the principle of protein-dye binding. Analytical Biochemistry **72**, 248-254.

Camino C, Gonzalez-Dugo V, Hernandez P, Sillero JC, Zarco-Tejada PJ. 2018. Improved nitrogen retrievals with airborne-derived fluorescence and plant traits quantified from VNIR-SWIR hyperspectral imagery in the context of precision agriculture. International Journal of Applied Earth Observation and Geoinformation **70**, 105-117.

Camino C, Gonzalez-Dugo V, Hernandez P, Zarco-Tejada PJ. 2019. Radiative transfer Vcmax estimation from hyperspectral imagery and SIF retrievals to assess photosynthetic performance in rainfed and irrigated plant phenotyping trials. Remote Sensing of Environment **231**, 111186.

Carmo-Silva E, Andralojc PJ, Scales JC, Driever SM, Mead A, Lawson T, Raines CA, Parry MAJ. 2017. Phenotyping of field-grown wheat in the UK highlights contribution of light response of photosynthesis and flag leaf longevity to grain yield. Journal of Experimental Botany **68**, 3473-3486.

Chapman EA, Orford S, Lage J, Griffiths S. 2021. Capturing and selecting senescence variation in wheat. Frontiers in Plant Science **12**, 638738.

Christopher M, Chenu K, Jennings R, Fletcher S, Butler D, Borrell A, Christopher J. 2018. QTL for stay-green traits in wheat in well-watered and water-limited environments. Field Crops Research **217**, 32-44.

Costa C, Schurr U, Loreto F, Menesatti P, Carpentier S. 2018. Plant phenotyping research trends, a science mapping approach. Frontiers in Plant Science **9**, 1933.

Dai J, Gao H, Dai Y, Zou Q. 2004. Changes in activity of energy dissipating mechanisms in wheat flag leaves during senescence. Plant Biology (Stuttg) **6**, 171-177.

Demidchik VV, Shashko AY, Bandarenka UY *et al*. 2020. Plant phenomics: fundamental bases, software and hardware platforms, and machine learning. Russian Journal of Plant Physiology **67**, 397-412.

Dobrowski SZ, Pushnik JC, Zarco-Tejada PJ, Ustin SL. 2005. Simple reflectance indices track heat and water stress-induced changes in steady-state chlorophyll fluorescence at the canopy scale. Remote Sensing of Environment **97**, 403-414.

Driever SM, Lawson T, Andralojc PJ, Raines CA, Parry MA. 2014. Natural variation in photosynthetic capacity, growth, and yield in 64 field-grown wheat genotypes. Journal of Experimental Botany **65**, 4959-4973.

Dwivedi SL, Scheben A, Edwards D, Spillane C, Ortiz R. 2017. Assessing and exploiting functional diversity in germplasm pools to enhance abiotic stress adaptation and yield in cereals and food legumes. Frontiers in Plant Science **8**, 1461.

Ethier GJ, Livingston NJ. 2004. On the need to incorporate sensitivity to CO2 transfer conductance into the Farquhar-von Caemmerer-Berry leaf photosynthesis model. Plant Cell and Environment **27**, 137-153.

FAO. 2017. The future of food and agriculture – Trends and challenges. Rome, Italy. http://www.fao.org/3/a-i6583e.pdf

Furbank RT, Tester M. 2011. Phenomics--technologies to relieve the phenotyping bottleneck. Trends in Plant Science **16**, 635-644.

Gamon JA, Field CB, Goulden ML, Griffin KL, Hartley AE, Joel G, Penuelas J, Valentini R. 1995. Relationships between NDVI, canopy structure, and photosynthesis in 3 Californian vegetation types. Ecological Applications **5**, 28-41.

Genty B, Briantais JM, Baker NR. 1989. The relationship between the quantum yield of photosynthetic electron-transport and quenching of chlorophyll fluorescence. Biochimica Et Biophysica Acta **990**, 87-92.

Gitelson AA, Gritz Y, Merzlyak MN. 2003. Relationships between leaf chlorophyll content and spectral reflectance and algorithms for non-destructive chlorophyll assessment in higher plant leaves. Journal of Plant Physiology **160**, 271-282.

Gitelson AA, Merzlyak MN. 1998. Remote sensing of chlorophyll concentration in higher plant leaves. Advances in Space Research **22**, 689-692.

Gonzalez-Dugo V, Hernandez P, Solis I, Zarco-Tejada PJ. 2015. Using high-resolution hyperspectral and thermal airborne imagery to assess physiological condition in the context of wheat phenotyping. Remote Sensing **7**, 13586-13605.

Grosskinsky DK, Pieruschka R, Svensgaard J, Rascher U, Christensen S, Schurr U, Roitsch T. 2015. Phenotyping in the fields: dissecting the genetics of quantitative traits and digital farming. New Phytologist **207**, 950-952.

Hailemichael G, Catalina A, Gonzalez MR, Martin P. 2016. Relationships between water status, leaf chlorophyll content and photosynthetic performance in tempranillo vineyards. South African Journal of Enology and Viticulture **37**, 149-156.

Hassan MA, Yang M, Rasheed A, Tian X, Reynolds M, Xia X, Xiao Y, He Z. 2021. Quantifying senescence in bread wheat using multispectral imaging from an unmanned aerial vehicle and QTL mapping. Plant Physiology **187**, 2623-2636.

Haworth M, Marino G, Centritto M. 2018. An introductory guide to gas exchange analysis of photosynthesis and its application to plant phenotyping and precision irrigation to enhance water use efficiency. Journal of Water and Climate Change **9**, 786-808.

Herritt MT, Pauli D, Mockler TC, Thompson AL. 2020. Chlorophyll fluorescence imaging captures photochemical efficiency of grain sorghum (Sorghum bicolor) in a field setting. Plant Methods **16**, 109.

Ishida A, Yamazaki JY, Harayama H *et al*. 2014. Photoprotection of evergreen and drought-deciduous tree leaves to overcome the dry season in monsoonal tropical dry forests in Thailand. Tree Physiology **34**, 15-28.

Jalink H, Schoor Rvd. 2011. Led induced chlorophyll fluorescence transient imager for measurements of health and stress status of whole plants. Proceedings of the International Symposium on High Technology for Greenhouse Systems: GreenSys2009, Quebec, Canada, June 14–19, 2009, **893**, 307-315.

Jia M, Li D, Colombo R *et al*. 2019. Quantifying chlorophyll fluorescence parameters from hyperspectral reflectance at the leaf scale under various nitrogen treatment regimes in winter wheat. Remote Sensing **11**, 2838.

Jones H, Vaughan R. 2010. Remote sensing of vegetation principles, techniques, and applications. Oxford University Press.

Kong L, Sun M, Xie Y, Wang F, Zhao Z. 2015. Photochemical and antioxidative responses of the glume and flag leaf to seasonal senescence in wheat. Frontiers in Plant Science **6**, 358.

Korres NE, Norsworthy JK, Tehranchian P *et al*. 2016. Cultivars to face climate change effects on crops and weeds: a review. Agronomy for Sustainable Development **36**, 12.

Kumari M, Patel NR, Raj R, Saha SK, Dadhwal VK. 2012. Parametric estimation of net photosynthesis in rice from in-situ spectral reflectance measurements. Current Science **103**, 55-61.

Letts MG, Phelan CA, Johnson DR, Rood SB. 2008. Seasonal photosynthetic gas exchange and leaf reflectance characteristics of male and female cottonwoods in a riparian woodland. Tree Physiology **28**, 1037-1048.

Li Q, Yang H, Guo J, Huang Q, Zhong S, Tan F, Ren T, Li Z, Chen C, Luo P. 2022. Comparative transcriptome analysis revealed differential gene expression involved in wheat leaf senescence between stay-green and non-stay-green cultivars. Frontiers in Plant Science **13**, 971927.

Long SP, Marshall-Colon A, Zhu XG. 2015. Meeting the global food demand of the future by engineering crop photosynthesis and yield potential. Cell **161**, 56-66.

Mackintosh CA, Garvin DF, Radmer LE, Heinen SJ, Muehlbauer GJ. 2006. A model wheat cultivar for transformation to improve resistance to Fusarium Head Blight. Plant Cell Reports **25**, 313-319.

Marshall B, Biscoe PV. 1980. A model for C3 leaves describing the dependence of net photosynthesis on irradiance. Journal of Experimental Botany **31**, 29-39.

McAusland L, Davey PA, Kanwal N, Baker NR, Lawson T. 2013. A novel system for spatial and temporal imaging of intrinsic plant water use efficiency Journal of Experimental Botany **64**, 4993-5007.

Meacham-Hensold K, Montes CM, Wu J *et al*. 2019. High-throughput field phenotyping using hyperspectral reflectance and partial least squares regression (PLSR) reveals genetic modifications to photosynthetic capacity. Remote Sensing of Environment **231**, 111176.

Merlier E, Hmimina G, Dufrene E, Soudani K. 2015. Explaining the variability of the photochemical reflectance index (PRI) at the canopy-scale: Disentangling the effects of phenological and physiological changes. Journal of Photochemistry and Photobiology B: Biology **151**, 161-171.

Misson L, Tu KP, Boniello RA, Goldstein AH. 2006. Seasonality of photosynthetic parameters in a multi-specific and vertically complex forest ecosystem in the Sierra Nevada of California. Tree Physiology **26**, 729-741.

Monteith JL. 1991. Plant and crop modelling--A mathematical approach to plant and crop physiology. Oxford: Clarendon Press.

Monteith JL, Moss CJ, Cooke GW, Pirie NW, Bell GDH. 1977. Climate and the efficiency of crop production in Britain. Philosophical Transactions of the Royal Society of London. B, Biological Sciences **281**, 277-294.

Montes CM, Fox C, Sanz-Saez A *et al*. 2022. High-throughput characterization, correlation, and mapping of leaf photosynthetic and functional traits in the soybean (Glycine max) nested association mapping population. Genetics **221,** iyac065.

Mu H, Jiang D, Wollenweber B, Dai T, Jing Q, Cao W. 2010. Long-term low radiation decreases leaf photosynthesis, photochemical efficiency and grain yield in winter wheat. Journal of Agronomy and Crop Science **196**, 38-47.

Murchie EH, Lawson T. 2013. Chlorophyll fluorescence analysis: a guide to good practice and understanding some new applications. Journal of Experimental Botany **64**, 3983-3998.

Pask A, Pietragalla J, Mullan D, Reynolds MP. 2012. Physiological Breeding II: A Field Guide to

Wheat Phenotyping. CIMMYT.

Pauli D, Chapman SC, Bart R, Topp CN, Lawrence-Dill CJ, Poland J, Gore MA. 2016. The quest for understanding phenotypic variation via integrated approaches in the field environment. Plant Physiology **172**, 622-634.

Peng J, Feng Y, Wang X, Li J, Xu G, Phonenasay S, Luo Q, Han Z, Lu W. 2021. Effects of nitrogen application rate on the photosynthetic pigment, leaf fluorescence characteristics, and yield of indica hybrid rice and their interrelations. Scientific Reports **11**, 7485.

Peng Y, Zeng AL, Zhu TG, Fang SH, Gong Y, Tao YQ, Zhou Y, Liu K. 2017. Using remotely sensed spectral reflectance to indicate leaf photosynthetic efficiency derived from active fluorescence measurements. Journal of Applied Remote Sensing **11**, 026034.

Pinto RS, Lopes MS, Collins NC, Reynolds MP. 2016. Modelling and genetic dissection of staygreen under heat stress. Theoretical and Applied Genetics **129**, 2055-2074.

Porcar-Castell A, Tyystjarvi E, Atherton J, van der Tol C, Flexas J, Pfundel EE, Moreno J, Frankenberg C, Berry JA. 2014. Linking chlorophyll a fluorescence to photosynthesis for remote sensing applications: mechanisms and challenges. Journal of Experimental Botany **65**, 4065-4095.

Reynolds M, Foulkes J, Furbank R, Griffiths S, King J, Murchie E, Parry M, Slafer G. 2012. Achieving yield gains in wheat. Plant Cell and Environment **35**, 1799-1823.

Reynolds M, Langridge P. 2016. Physiological breeding. Current Opinion in Plant Biology **31**, 162-171.

Sadeghi-Tehran P, Virlet N, Hawkesford MJ. 2021. A neural network method for classification of sunlit and shaded components of wheat canopies in the field using high-resolution hyperspectral imagery. Remote Sensing **13**, 898.

Scheben A, Yuan YX, Edwards D. 2016. Advances in genomics for adapting crops to climate change. Current Plant Biology **6**, 2-10.

Shao GQ, Li ZJ, Ning TY, Zheng YH. 2013. Responses of photosynthesis, chlorophyll fluorescence, and grain yield of maize to controlled-release urea and irrigation after anthesis. Journal of Plant Nutrition and Soil Science **176**, 595-602.

Shunmugam ASK, Kannan U, Jiang Y, Daba KA, Gorim LY. 2018. Physiology based approaches for breeding of next-generation food legumes. Plants (Basel) **7**, 72.

Silva-Perez V, Molero G, Serbin SP, Condon AG, Reynolds MP, Furbank RT, Evans JR. 2018. Hyperspectral reflectance as a tool to measure biochemical and physiological traits in wheat. Journal of Experimental Botany **69**, 483-496.

Sreeman SM, Vijayaraghavareddy P, Sreevathsa R, Rajendrareddy S, Arakesh S, Bharti P, Dharmappa P, Soolanayakanahally R. 2018. Introgression of physiological traits for a comprehensive improvement of drought adaptation in crop plants. Frontiers in Chemistry **6**, 92.

Sun J, Feng Z, Ort DR. 2014. Impacts of rising tropospheric ozone on photosynthesis and metabolite levels on field grown soybean. Plant Science **226**, 147-161.

Tan CW, Huang WJ, Jin XL, Wang JC, Tong L, Wang JH, Guo WS. 2012. Monitoring the Chlorophyll Fluorescence Parameter F-v/F-m in Compact Corn Based on Different Hyperspectral Vegetation Indices. Spectroscopy and Spectral Analysis **32**, 1287-1291.

R Core Team. 2020. A language and environment for statistical computing. Vienna, Austria: R Foundation for Statistical Computing. https:\\www.r-project.org (accessed on 14 Febuary 2019).

Thomas H, Howarth CJ. 2000. Five ways to stay green Journal of Experimental Botany **51**, 329-337.

Thomas H, Ougham H. 2014. The stay-green trait. Journal of Experimental Botany **65**, 3889-3900.

Thornley JH, Johnson IR. 1990. Plant and crop modelling. Oxford: Clarendon Press.

Urban MO, Klima M, Vitamvas P, Vasek J, Hilgert-Delgado AA, Kucera V. 2013. Significant relationships among frost tolerance and net photosynthetic rate, water use efficiency and dehydrin accumulation in cold-treated winter oilseed rapes. Journal of Plant Physiology **170**, 1600-1608.

van Bezouw R, Keurentjes JJB, Harbinson J, Aarts MGM. 2019. Converging phenomics and genomics to study natural variation in plant photosynthetic efficiency. Plant Journal **97**, 112-133.

Virlet N, Lyra DH, Hawkesford MJ. 2022. Digital phenotyping and genotype-to-phenotype (G2P) models to predict complex traits in cereal crops. In: Burleigh Dodds Science Publishing. Advances in plant phenotyping for more sustainable crop production, **223-262**.

Virlet N, Sabermanesh K, Sadeghi-Tehran P, Hawkesford MJ. 2016. Field Scanalyzer: An automated robotic field phenotyping platform for detailed crop monitoring. Functional Plant Biology **44**, 143-153.

Whitney SM, von Caemmerer S, Hudson GS, Andrews TJ. 1999. Directed mutation of the Rubisco large subunit of tobacco influences photorespiration and growth. Plant Physiology **121**, 579-588.

Wintermans JFGM, De Mots A. 1965. Spectrophotometric characteristics of chlorophylls a and b and their phenophytins in ethanol. Biochimica et Biophysica Acta (BBA) - Biophysics including Photosynthesis **109**, 448-453.

Wyber R, Osmond B, Ashcroft MB, Malenovsky Z, Robinson SA. 2018. Remote monitoring of dynamic canopy photosynthesis with high time resolution light-induced fluorescence transients. Tree Physiology **38**, 1302-1318.

Xu JK, Shi Y, Yu ZW, Zhao JY. 2017. Irrigation methods affect wheat flag leaf senescence and chlorophyll fluorescence in the North China Plain. International Journal of Plant Production **11**, 361-377.

Yang W, Feng H, Zhang X, Zhang J, Doonan JH, Batchelor WD, Xiong L, Yan J. 2020. Crop phenomics and high-throughput phenotyping: past decades, current challenges, and future perspectives. Molecular Plant **13**, 187-214.

York LM. 2019. Functional phenomics: an emerging field integrating high-throughput phenotyping, physiology, and bioinformatics. Journal of Experimental Botany **70**, 379-386.

Zarco-Tejada PJ, Berjon A, Lopez-Lozano R, Miller JR, Martin P, Cachorro V, Gonzalez MR, de Frutos A. 2005. Assessing vineyard condition with hyperspectral indices: Leaf and canopy reflectance simulation in a row-structured discontinuous canopy. Remote Sensing of Environment **99**, 271-287.

Zarco-Tejada PJ, Catalina A, Gonzalez MR, Martin P. 2013. Relationships between net photosynthesis and steady-state chlorophyll fluorescence retrieved from airborne hyperspectral imagery. Remote Sensing of Environment **136**, 247-258.

Zhao C, Zhang Y, Du J, Guo X, Wen W, Gu S, Wang J, Fan J. 2019. Crop phenomics: current status and perspectives. Frontiers in Plant Science **10**, 714.

Zhou Y, Ju W, Sun X, Hu Z, Han S, Black TA, Jassal RS, Wu X. 2014. Close relationship between spectral vegetation indices and Vcmax in deciduous and mixed forests. Tellus B: Chemical and Physical Meteorology **66**, 23279.

Zhu XG, Long SP, Ort DR. 2010. Improving photosynthetic efficiency for greater yield. Annual Review of Plant Biology **61**, 235-261.

Zhuang J, Wang Y, Chi Y, Zhou L, Chen J, Zhou W, Song J, Zhao N, Ding J. 2020. Drought stress strengthens the link between chlorophyll fluorescence parameters and photosynthetic traits. PeerJ

8, e10046 doi.org/10.7717/peerj.10046

Wyber, R., B. Osmond, M. B. Ashcroft, Z. Malenovsky and S. A. Robinson (2018). Remote monitoring of dynamic canopy photosynthesis with high time resolution light-induced fluorescence transients. Tree Physiol 38(9): 1302-1318. DOI: 10.1093/treephys/tpx161.

Xu, J. K., Y. Shi, Z. W. Yu and J. Y. Zhao (2017). Irrigation methods affect wheat flag leaf senescence and chlorophyll fluorescence in the North China Plain. International Journal of Plant Production 11(3): 361-377. DOI: 10.22069/ijpp.2017.3545.

Yang, W., H. Feng, X. Zhang, J. Zhang, J. H. Doonan, W. D. Batchelor, L. Xiong and J. Yan (2020). Crop Phenomics and High-Throughput Phenotyping: Past Decades, Current Challenges, and Future Perspectives. Mol Plant 13(2): 187-214. DOI: 10.1016/j.molp.2020.01.008.

York, L. M. (2019). Functional phenomics: an emerging field integrating high-throughput phenotyping, physiology, and bioinformatics. J Exp Bot 70(2): 379-386. DOI: 10.1093/jxb/ery379.

Zarco-Tejada, P. J., A. Berjon, R. Lopez-Lozano, J. R. Miller, P. Martin, V. Cachorro, M. R. Gonzalez and A. de Frutos (2005). Assessing vineyard condition with hyperspectral indices: Leaf and canopy reflectance simulation in a row-structured discontinuous canopy. Remote Sensing of Environment 99(3): 271-287. DOI: 10.1016/j.rse.2005.09.002.

Zarco-Tejada, P. J., A. Catalina, M. R. Gonzalez and P. Martin (2013). Relationships between net photosynthesis and steady-state chlorophyll fluorescence retrieved from airborne hyperspectral imagery. Remote Sensing of Environment 136: 247-258. DOI: 10.1016/j.rse.2013.05.011.

Zhao, C., Y. Zhang, J. Du, X. Guo, W. Wen, S. Gu, J. Wang and J. Fan (2019). Crop Phenomics: Current Status and Perspectives. Front Plant Sci 10: 714. DOI: 10.3389/fpls.2019.00714.

Zhou, Y., W. Ju, X. Sun, Z. Hu, S. Han, T. A. Black, R. S. Jassal and X. Wu (2014). Close relationship between spectral vegetation indices and Vcmax in deciduous and mixed forests. Tellus B: Chemical and Physical Meteorology 66(1): 23279. DOI: 10.3402/tellusb.v66.23279.

Zhu, X. G., S. P. Long and D. R. Ort (2010). Improving photosynthetic efficiency for greater yield. Annu Rev Plant Biol 61: 235-261. DOI: 10.1146/annurev-arplant-042809-112206.

Zhuang, J., Y. Wang, Y. Chi, L. Zhou, J. Chen, W. Zhou, J. Song, N. Zhao and J. Ding (2020). Drought stress strengthens the link between chlorophyll fluorescence parameters and photosynthetic traits. PeerJ 8: e10046. DOI: 10.7717/peerj.10046.

Tables

Table 1. Parameters of linear regressions between chlorophyll fluorescence (F_v/F_m) measured by the Field Scanalyzer and other measured parameters

Parameters			Bobwhite			Cadenza			Generalist Model			Interaction Model							
y		x	F	*p*	R^2_{adj}	F	*p*	R^2_{adj}	F	*p*	R^2_{adj}	F (Par.)	*p* (Par.)	F (cv..)	*p* (cv..)	F (Int.)	*p* (Int.)	*p* (Mod.)	R^2_{adj}
V_{cmax}	*vs*	F_v/F_mSc	12.7	0.003	0.46	17.9	0.001	0.55	12.8	0.001	0.29	18.3	0.000	14.2	0.001	0.0	0.954	0.000	0.50
J	*vs*	F_v/F_mSc	14.3	0.002	0.49	20.7	0.001	0.58	17.6	0.000	0.36	24.5	0.000	12.9	0.001	0.0	0.858	0.000	0.54
g_m	*vs*	F_v/F_mSc	22.5	0.000	0.61	17.1	0.001	0.54	25.3	0.000	0.46	31.3	0.000	6.9	0.014	1.7	0.202	0.000	0.56
k_c^c	*vs*	F_v/F_mSc	7.6	0.016	0.32	7.9	0.015	0.33	11.5	0.002	0.27	12.2	0.002	3.6	0.067	0.0	0.892	0.006	0.31
$R_{photoresp}$	*vs*	F_v/F_mSc	16.8	0.001	0.53	16.3	0.001	0.52	29.4	0.000	0.49	31.6	0.000	4.0	0.055	0.0	0.916	0.000	0.53
A_{max}	*vs*	F_v/F_mSc	13.2	0.003	0.47	19.1	0.001	0.56	44.8	0.000	0.60	43.0	0.000	0.9	0.365	0.0	0.943	0.000	0.58
TSP	*vs*	F_v/F_mSc	19.5	0.001	0.57	23.3	0.000	0.61	18.4	0.000	0.38	27.8	0.000	16.3	0.000	0.0	0.827	0.000	0.59
Chl a	*vs*	F_v/F_mSc	0.1	0.767	-0.07	18.3	0.001	0.55	5.3	0.029	0.13	8.7	0.007	13.6	0.001	6.0	0.021	0.000	0.47
Chl b	*vs*	F_v/F_mSc	0.8	0.392	-0.02	7.8	0.015	0.33	0.8	0.386	-0.01	1.1	0.297	9.5	0.005	5.3	0.030	0.006	0.31
Rubisco	*vs*	F_v/F_mSc	5.4	0.037	0.24	11.6	0.005	0.43	12.9	0.001	0.29	14.1	0.001	4.5	0.043	0.0	0.878	0.003	0.35
V_i	*vs*	F_v/F_mSc	13.5	0.003	0.47	42.6	0.000	0.75	32.0	0.000	0.52	45.0	0.000	13.3	0.001	0.1	0.736	0.000	0.66
V_t	*vs*	F_v/F_mSc	24.3	0.000	0.62	30.7	0.000	0.68	19.6	0.000	0.39	34.2	0.000	22.7	0.000	0.1	0.725	0.000	0.65
SPAD	*vs*	F_v/F_mSc	0.7	0.407	-0.02	13.1	0.003	0.46	1.0	0.331	0.00	1.9	0.181	25.4	0.000	2.8	0.104	0.000	0.48
Φ(II)FP	*vs*	F_v/F_mSc	6.8	0.022	0.29	9.8	0.008	0.39	31.7	0.000	0.51	30.2	0.000	0.1	0.723	0.5	0.493	0.000	0.49
Φ(II)FM	*vs*	F_v/F_mSc	2.4	0.145	0.09	26.0	0.000	0.64	11.0	0.003	0.26	16.1	0.000	12.7	0.001	2.1	0.155	0.000	0.49
Φ(II)HP	*vs*	F_v/F_mSc	2.5	0.136	0.10	26.6	0.000	0.65	28.2	0.000	0.48	26.3	0.000	0.0	0.980	0.0	0.834	0.000	0.45
F_v/F_mHP	*vs*	F_v/F_mSc	11.7	0.005	0.43	25.0	0.000	0.63	60.3	0.000	0.67	56.1	0.000	0.0	0.863	0.0	0.946	0.000	0.65

y and x, elements of the regression; *p* (Eq), p-value of the regression; R^2_{adj}, adjusted coefficient of determination of the regression; *p* (Eq) < 0.05, the regression is significant (rows in black);

Table 2. Parameters of linear regressions between the normalized difference vegetation index (NDVI) measured by the Field Scanalyzer and other measured parameters

Parameters			Bobwhite			Cadenza			Gen. Model			Line effect							
y		x	F	*p*	R^2_{adj}	F	*p*	R^2_{adj}	F	*p*	R^2_{adj}	F (Par.)	*p* (Par.)	F (cv.)	*p* (cv.)	F (Int.)	*p* (Int.)	*p* (Eq)	R^2_{adj}
V_{cmax}	*vs*	NDVI	0.7	0.405	-0.02	43.0	0.000	0.75	21.2	0.000	0.41	25.0	0.000	4.5	0.043	2.6	0.121	0.000	0.50
J	*vs*	NDVI	0.8	0.379	-0.01	74.0	0.000	0.84	31.6	0.000	0.51	38.2	0.000	3.8	0.063	4.1	0.053	0.000	0.60
g_m	*vs*	NDVI	1.2	0.302	0.01	18.3	0.001	0.55	16.3	0.000	0.35	15.3	0.001	0.1	0.794	0.3	0.587	0.006	0.30
k_c^c	*vs*	NDVI	1.2	0.298	0.01	36.4	0.000	0.72	27.3	0.000	0.48	28.1	0.000	1.1	0.307	1.8	0.188	0.000	0.49
$R_{photoresp}$	*vs*	NDVI	0.9	0.368	-0.01	23.2	0.000	0.61	24.9	0.000	0.45	24.7	0.000	0.0	0.954	1.7	0.202	0.000	0.45
A_{max}	*vs*	NDVI	0.9	0.352	-0.01	34.2	0.000	0.70	33.1	0.000	0.53	35.2	0.000	1.6	0.212	2.2	0.152	0.000	0.55
TSP	*vs*	NDVI	1.5	0.247	0.03	52.2	0.000	0.79	27.7	0.000	0.48	31.2	0.000	3.7	0.066	1.9	0.180	0.000	0.54
Chl a	*vs*	NDVI	3.1	0.101	0.13	13.3	0.003	0.47	6.6	0.016	0.16	9.5	0.005	5.0	0.035	9.4	0.005	0.001	0.42
Chl b	*vs*	NDVI	4.4	0.057	0.19	7.2	0.019	0.31	2.3	0.139	0.04	3.3	0.081	6.5	0.017	7.1	0.013	0.004	0.32
Rubisco	*vs*	NDVI	0.1	0.740	-0.07	37.0	0.000	0.72	20.0	0.000	0.40	21.8	0.000	0.8	0.369	3.7	0.065	0.000	0.45
V_i	*vs*	NDVI	0.4	0.564	-0.05	46.3	0.000	0.76	26.3	0.000	0.47	28.4	0.000	0.7	0.426	3.6	0.069	0.000	0.51
V_t	*vs*	NDVI	0.6	0.443	-0.03	49.2	0.000	0.78	22.0	0.000	0.42	25.5	0.000	3.8	0.062	2.7	0.110	0.000	0.50
SPAD	*vs*	NDVI	0.6	0.467	-0.03	14.6	0.002	0.49	3.9	0.059	0.09	7.1	0.013	18.7	0.000	6.4	0.017	0.000	0.50
Φ(II)FP	*vs*	NDVI	0.4	0.545	-0.05	11.2	0.005	0.42	18.9	0.000	0.38	22.0	0.000	4.6	0.042	2.0	0.170	0.000	0.47
Φ(II)FM	*vs*	NDVI	0.1	0.808	-0.07	29.9	0.000	0.67	14.3	0.001	0.32	18.7	0.000	3.6	0.069	6.8	0.015	0.000	0.47
Φ(II)HP	*vs*	NDVI	0.0	0.927	-0.08	13.0	0.003	0.46	9.6	0.004	0.23	10.5	0.003	3.2	0.084	1.3	0.261	0.007	0.29
F_v/F_mHP	*vs*	NDVI	0.6	0.466	-0.03	41.9	0.000	0.75	29.9	0.000	0.50	35.5	0.000	4.9	0.036	2.3	0.138	0.000	0.58

y and x, elements of the regression; *p* (Eq), p-value of the regression; R^2_{adj}, adjusted coefficient of determination of the regression; *p* (Eq) < 0.05, the regression is significant (rows in black);

Table 3. Parameters of linear regressions between chlorophyll fluorescence (F_v/F_m) measured by the Phenocenter and other measured parameters

Parameters			Bobwhite			Cadenza			Gen. Model			Line effect							
y		x	F	*p*	R^2_{adj}	F	*p*	R^2_{adj}	F	*p*	R^2_{adj}	F (Par.)	*p* (Par.)	F (cv.)	*p* (cv.)	F (Int.)	*p* (Int.)	*p* (Eq)	R^2_{adj}
V_{cmax}	*vs*	F_v/F_mPc	0.7	0.407	-0.02	44.3	0.000	0.76	32.1	0.000	0.52	31.3	0.000	0.2	0.662	1.1	0.308	0.000	0.50
J	*vs*	F_v/F_mPc	1.0	0.345	0.00	82.3	0.000	0.85	47.3	0.000	0.62	46.8	0.000	0.0	0.914	1.7	0.206	0.000	0.61
g_m	*vs*	F_v/F_mPc	0.1	0.756	-0.07	19.6	0.001	0.57	12.6	0.001	0.28	12.5	0.002	0.9	0.345	0.9	0.360	0.009	0.28
k_c^c	*vs*	F_v/F_mPc	0.0	0.923	-0.08	28.7	0.000	0.66	20.8	0.000	0.41	21.6	0.000	0.4	0.531	2.6	0.118	0.001	0.43
$R_{photoresp}$	*vs*	F_v/F_mPc	0.6	0.464	-0.03	28.2	0.000	0.66	23.7	0.000	0.44	25.3	0.000	2.8	0.108	1.1	0.304	0.000	0.47
A_{max}	*vs*	F_v/F_mPc	0.1	0.710	-0.07	42.7	0.000	0.75	21.1	0.000	0.41	28.9	0.000	9.8	0.004	2.5	0.129	0.000	0.57
TSP	*vs*	F_v/F_mPc	0.1	0.809	-0.07	45.4	0.000	0.76	27.1	0.000	0.47	27.8	0.000	0.0	0.949	2.8	0.109	0.000	0.49
Chl a	*vs*	F_v/F_mPc	7.5	0.017	0.32	11.8	0.004	0.44	23.1	0.000	0.43	22.5	0.000	1.3	0.272	0.0	0.921	0.001	0.42
Chl b	*vs*	F_v/F_mPc	5.6	0.035	0.25	8.4	0.012	0.35	15.2	0.001	0.33	16.1	0.000	3.5	0.071	0.0	0.957	0.002	0.36
Rubisco	*vs*	F_v/F_mPc	0.0	0.854	-0.07	31.0	0.000	0.68	18.6	0.000	0.38	19.9	0.000	0.3	0.562	3.6	0.070	0.001	0.42
V_i	*vs*	F_v/F_mPc	2.8	0.115	0.12	29.8	0.000	0.67	31.5	0.000	0.51	30.2	0.000	0.8	0.374	0.0	0.859	0.000	0.49
V_t	*vs*	F_v/F_mPc	1.5	0.246	0.03	46.1	0.000	0.76	34.9	0.000	0.54	33.0	0.000	0.1	0.797	0.4	0.523	0.000	0.51
SPAD	*vs*	F_v/F_mPc	0.2	0.681	-0.06	16.2	0.001	0.52	15.4	0.001	0.33	21.3	0.000	10.9	0.003	1.8	0.191	0.000	0.52
Φ(II)FP	*vs*	F_v/F_mPc	0.1	0.737	-0.07	14.8	0.002	0.50	12.6	0.001	0.29	18.6	0.000	13.6	0.001	1.8	0.188	0.000	0.52
Φ(II)FM	*vs*	F_v/F_mPc	3.0	0.105	0.13	61.6	0.000	0.81	54.8	0.000	0.65	52.2	0.000	0.2	0.623	0.4	0.529	0.000	0.63
Φ(II)HP	*vs*	F_v/F_mPc	12.4	0.004	0.45	25.2	0.000	0.63	17.9	0.000	0.37	28.4	0.000	13.4	0.001	4.9	0.035	0.000	0.60
F_v/F_mHP	*vs*	F_v/F_mPc	1.7	0.211	0.05	65.0	0.000	0.82	22.3	0.000	0.42	35.8	0.000	18.7	0.000	0.3	0.582	0.000	0.64

y and x, elements of the regression; *p* (Eq), p-value of the regression; R^2_{adj}, adjusted coefficient of determination of the regression; *p* (Eq) < 0.05, the regression is significant (rows in black);

Table 4. Parameters of linear regressions between photosystem II quantum efficiency ($\Phi(II)_{532}$) measured by the Phenocenter and other measured parameters

Parameters			Bobwhite			Cadenza			Gen. Model			Line effect							
y		x	F	*p*	R^2_{adj}	F	*p*	R^2_{adj}	F	*p*	R^2_{adj}	F (Par.)	*p* (Par.)	F (cv.)	*p* (cv.)	F (Int.)	*p* (Int.)	*p* (Eq)	R^2_{adj}
V_{cmax}	*vs*	$\Phi(II)_{532}$	19.2	0.001	0.57	34.0	0.000	0.70	23.5	0.000	0.44	37.8	0.000	17.6	0.000	1.4	0.244	0.000	0.65
J	*vs*	$\Phi(II)_{532}$	17.9	0.001	0.55	65.9	0.000	0.82	21.6	0.000	0.42	48.5	0.000	32.3	0.000	4.6	0.041	0.000	0.74
g_m	*vs*	$\Phi(II)_{532}$	15.4	0.002	0.51	26.6	0.000	0.65	9.9	0.004	0.23	18.0	0.000	24.9	0.000	0.0	0.850	0.000	0.58
k_c^c	*vs*	$\Phi(II)_{532}$	24.9	0.000	0.63	21.0	0.001	0.59	12.7	0.001	0.29	22.0	0.000	22.0	0.000	0.5	0.478	0.000	0.59
$R_{photoresp}$	*vs*	$\Phi(II)_{532}$	16.4	0.001	0.52	41.2	0.000	0.74	8.6	0.007	0.21	21.7	0.000	41.5	0.000	2.8	0.108	0.000	0.68
A_{max}	*vs*	$\Phi(II)_{532}$	9.0	0.010	0.36	73.2	0.000	0.84	3.9	0.057	0.09	13.4	0.001	64.0	0.000	5.5	0.027	0.000	0.73
TSP	*vs*	$\Phi(II)_{532}$	9.3	0.009	0.37	65.0	0.000	0.82	19.6	0.000	0.39	36.3	0.000	21.9	0.000	4.1	0.052	0.000	0.67
Chl a	*vs*	$\Phi(II)_{532}$	0.9	0.370	-0.01	13.0	0.003	0.46	7.0	0.013	0.17	9.5	0.005	1.0	0.328	11.4	0.002	0.001	0.39
Chl b	*vs*	$\Phi(II)_{532}$	3.2	0.095	0.14	7.5	0.017	0.32	5.7	0.024	0.14	7.2	0.012	0.1	0.802	9.6	0.005	0.004	0.32
Rubisco	*vs*	$\Phi(II)_{532}$	4.2	0.061	0.19	30.9	0.000	0.68	9.4	0.005	0.22	14.7	0.001	14.8	0.001	3.0	0.094	0.000	0.50
V_i	*vs*	$\Phi(II)_{532}$	6.3	0.026	0.27	43.1	0.000	0.75	10.3	0.003	0.24	19.3	0.000	22.7	0.000	3.8	0.062	0.000	0.60
V_t	*vs*	$\Phi(II)_{532}$	7.3	0.018	0.31	69.7	0.000	0.83	20.1	0.000	0.40	34.8	0.000	18.3	0.000	4.3	0.048	0.000	0.65
SPAD	*vs*	$\Phi(II)_{532}$	0.3	0.609	-0.05	21.6	0.000	0.60	18.9	0.000	0.38	27.2	0.000	0.1	0.713	14.2	0.001	0.000	0.57
Φ(II)FP	*vs*	$\Phi(II)_{532}$	6.5	0.024	0.28	7.2	0.019	0.31	0.2	0.623	-0.03	0.4	0.510	23.6	0.000	1.2	0.281	0.000	0.43
Φ(II)FM	*vs*	$\Phi(II)_{532}$	2.6	0.132	0.10	47.0	0.000	0.77	15.6	0.000	0.34	25.4	0.000	11.3	0.002	8.2	0.008	0.000	0.59
Φ(II)HP	*vs*	$\Phi(II)_{532}$	0.9	0.371	-0.01	25.5	0.000	0.64	0.4	0.545	-0.02	0.6	0.435	19.2	0.000	1.9	0.184	0.001	0.39

F_v/F_mHP	*vs*	$\Phi(II)_{532}$	8.3	0.013	0.34	131.7	0.000	0.90	2.2	0.153	0.04	8.9	0.006	84.4	0.000	4.7	0.040	0.000	0.77

y and x, elements of the regression; *p* (Eq), p-value of the regression; R^2_{adj}, adjusted coefficient of determination of the regression; *p* (Eq) < 0.05, the regression is significant (rows in black);

Table 5. Parameters of linear regressions between non-photochemical quenching ($\Phi(NPQ)_{1077}$) measured by the Phenocenter and other measured parameters

Parameters			Bobwhite			Cadenza			Gen. Model			Line effect							
y		x	F	*p*	R^2_{adj}	F	*p*	R^2_{adj}	F	*p*	R^2_{adj}	F (Par.)	*p* (Par.)	F (cv.)	*p* (cv.)	F (Int.)	*p* (Int.)	*p* (Eq)	R^2_{adj}
V_{cmax}	*vs*	$\Phi(NPQ)_{1077}$	63.6	0.000	0.82	6.0	0.031	0.28	16.8	0.000	0.36	20.8	0.000	7.9	0.009	0.4	0.544	0.000	0.48
J	*vs*	$\Phi(NPQ)_{1077}$	75.7	0.000	0.84	13.5	0.003	0.49	30.0	0.000	0.51	36.5	0.000	7.7	0.010	0.1	0.743	0.000	0.60
g_m	*vs*	$\Phi(NPQ)_{1077}$	101.2	0.000	0.88	3.6	0.084	0.16	25.2	0.000	0.46	27.1	0.000	1.1	0.306	3.0	0.096	0.000	0.50
k_c^c	*vs*	$\Phi(NPQ)_{1077}$	50.2	0.000	0.78	4.0	0.069	0.19	17.3	0.000	0.37	17.3	0.000	1.6	0.217	0.3	0.583	0.002	0.37
$R_{photoresp}$	*vs*	$\Phi(NPQ)_{1077}$	112.5	0.000	0.89	5.1	0.043	0.24	26.3	0.000	0.47	24.8	0.000	0.2	0.634	0.2	0.651	0.000	0.44
A_{max}	*vs*	$\Phi(NPQ)_{1077}$	55.8	0.000	0.80	12.5	0.004	0.47	49.3	0.000	0.63	46.7	0.000	0.5	0.495	0.1	0.782	0.000	0.61
TSP	*vs*	$\Phi(NPQ)_{1077}$	20.9	0.001	0.59	12.0	0.005	0.46	21.3	0.000	0.42	24.2	0.000	5.4	0.029	0.3	0.612	0.000	0.49
Chl a	*vs*	$\Phi(NPQ)_{1077}$	0.0	0.852	-0.07	4.4	0.057	0.21	1.1	0.300	0.00	1.4	0.248	4.9	0.037	3.8	0.061	0.034	0.20
Chl b	*vs*	$\Phi(NPQ)_{1077}$	1.5	0.241	0.04	2.5	0.141	0.10	0.0	0.935	-0.04	0.0	0.926	6.3	0.019	3.9	0.059	0.034	0.20
Rubisco	*vs*	$\Phi(NPQ)_{1077}$	9.0	0.010	0.36	8.1	0.015	0.35	15.7	0.000	0.34	15.5	0.001	1.2	0.276	0.3	0.560	0.004	0.33
V_i	*vs*	$\Phi(NPQ)_{1077}$	24.1	0.000	0.62	9.1	0.011	0.38	24.3	0.000	0.45	24.1	0.000	1.8	0.193	0.0	0.855	0.000	0.45
V_t	*vs*	$\Phi(NPQ)_{1077}$	44.4	0.000	0.76	10.4	0.007	0.42	23.1	0.000	0.44	27.9	0.000	7.6	0.011	0.0	0.961	0.000	0.54
SPAD	*vs*	$\Phi(NPQ)_{1077}$	0.8	0.398	-0.02	12.6	0.004	0.47	2.1	0.161	0.04	4.2	0.050	24.0	0.000	6.0	0.022	0.000	0.53
$\Phi(II)FP$	*vs*	$\Phi(NPQ)_{1077}$	5.8	0.032	0.25	2.2	0.160	0.09	9.1	0.005	0.23	9.6	0.005	3.3	0.080	0.1	0.713	0.013	0.27
$\Phi(II)FM$	*vs*	$\Phi(NPQ)_{1077}$	4.8	0.047	0.21	11.7	0.005	0.45	9.8	0.004	0.24	11.9	0.002	6.3	0.019	1.4	0.247	0.002	0.37
$\Phi(II)HP$	*vs*	$\Phi(NPQ)_{1077}$	2.9	0.113	0.12	5.9	0.031	0.28	11.2	0.002	0.27	11.2	0.003	1.9	0.179	0.0	0.945	0.013	0.26
F_v/F_mHP	*vs*	$\Phi(NPQ)_{1077}$	26.5	0.000	0.65	16.2	0.002	0.54	49.4	0.000	0.63	51.7	0.000	3.1	0.089	0.1	0.733	0.000	0.65

y and x, elements of the regression; *p* (Eq), p-value of the regression; R^2_{adj}, adjusted coefficient of determination of the regression; *p* (Eq) < 0.05, the regression is significant (rows in black);

Figure legends

Fig. 1. Example Phenocenter images for chlorophyll fluorescence (F_v/F_m) and photosystem II quantum efficiency ($\Phi(II)$) analysis. $\Phi(II)_X$, photosystem II quantum efficiency at the light level of X µmols photons m^{-2} s^{-1}.

Fig. 2. Example Field Scanalyzer images for chlorophyll fluorescence (F_v/F_mSc). Z4.5, booting stage; Z6.5, anthesis; Z6.5 + 7d, 7 days post-anthesis; Z6.5 + 14d, 14 days post-anthesis; Z6.5 + 21d, 21 days post-anthesis.

Fig. 3. Mean and standard deviation for each variable for Bobwhite (orange) and Cadenza (blue) at booting (Z4.5), anthesis (Z6.5) and at 7-, 14- and 21-days post anthesis (Z6.5+7, +14, +21) for (A) gas-exchange, (B) biochemical, (C), handheld devices and, (D) image variables. Letters come from the post-hoc test *HSD.test* allowing multiple comparisons of treatments (here time point and cultivar) by means of Tukey. Different letters indicate a statistical difference between cultivar and/or date (a = 0.05).

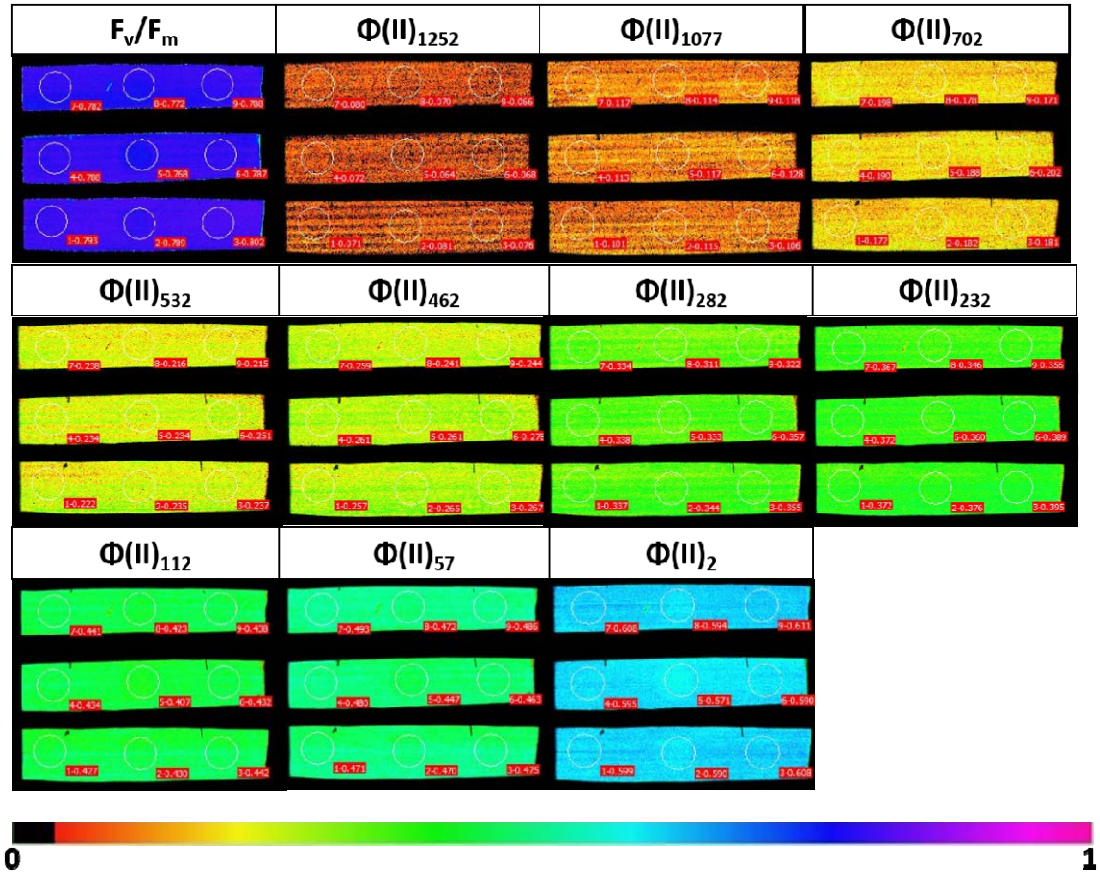

Fig. 1. Example Phenocenter images for chlorophyll fluorescence (F_v/F_m) and photosystem II quantum efficiency (Φ(II)) analysis. $\Phi(II)_X$, photosystem II quantum efficiency at the light level of X µmols photons m^{-2} s^{-1}.

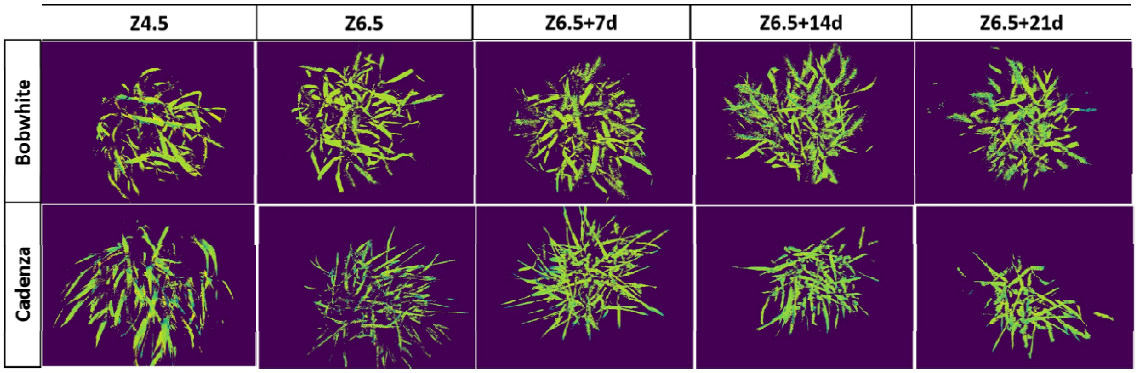

Fig. 2. Example Field Scanalyzer images for chlorophyll fluorescence (F_v/F_mSc). Z4.5, booting stage; Z6.5, anthesis; Z6.5 + 7d, 7 days post-anthesis; Z6.5 + 14d, 14 days post-anthesis; Z6.5 + 21d, 21 days post-anthesis.

A – Gas-exchange

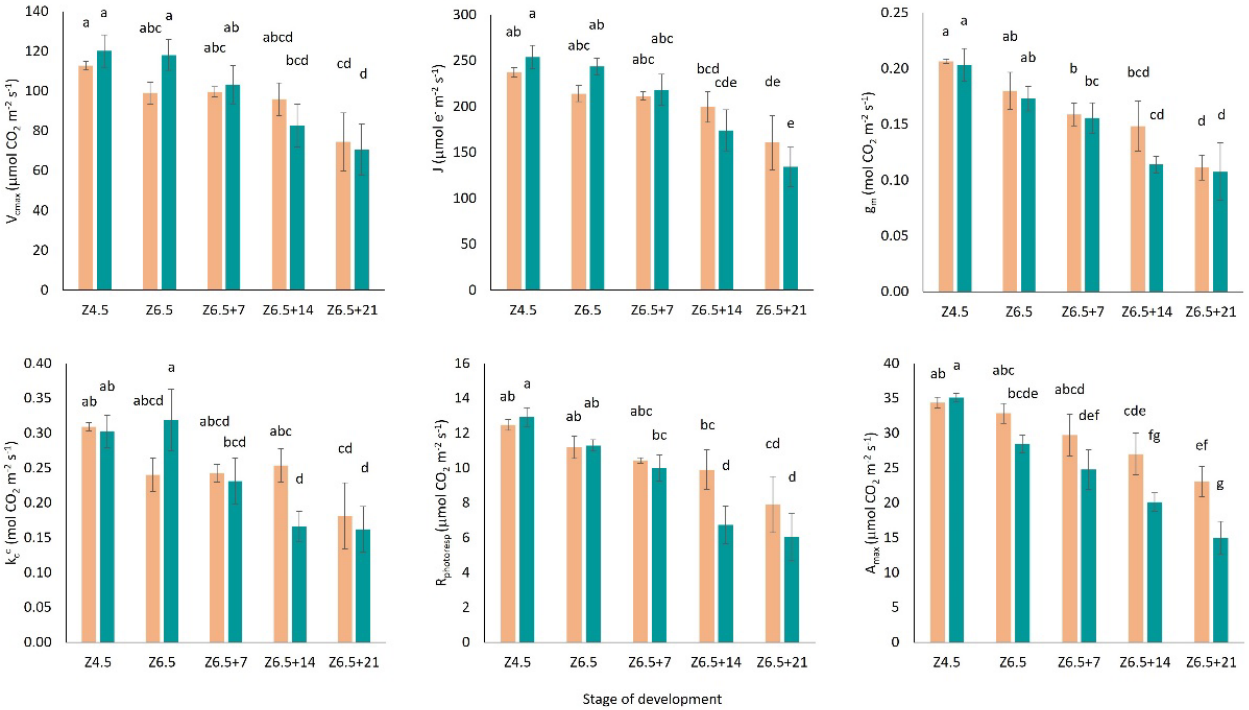

B – Biochemical analysis

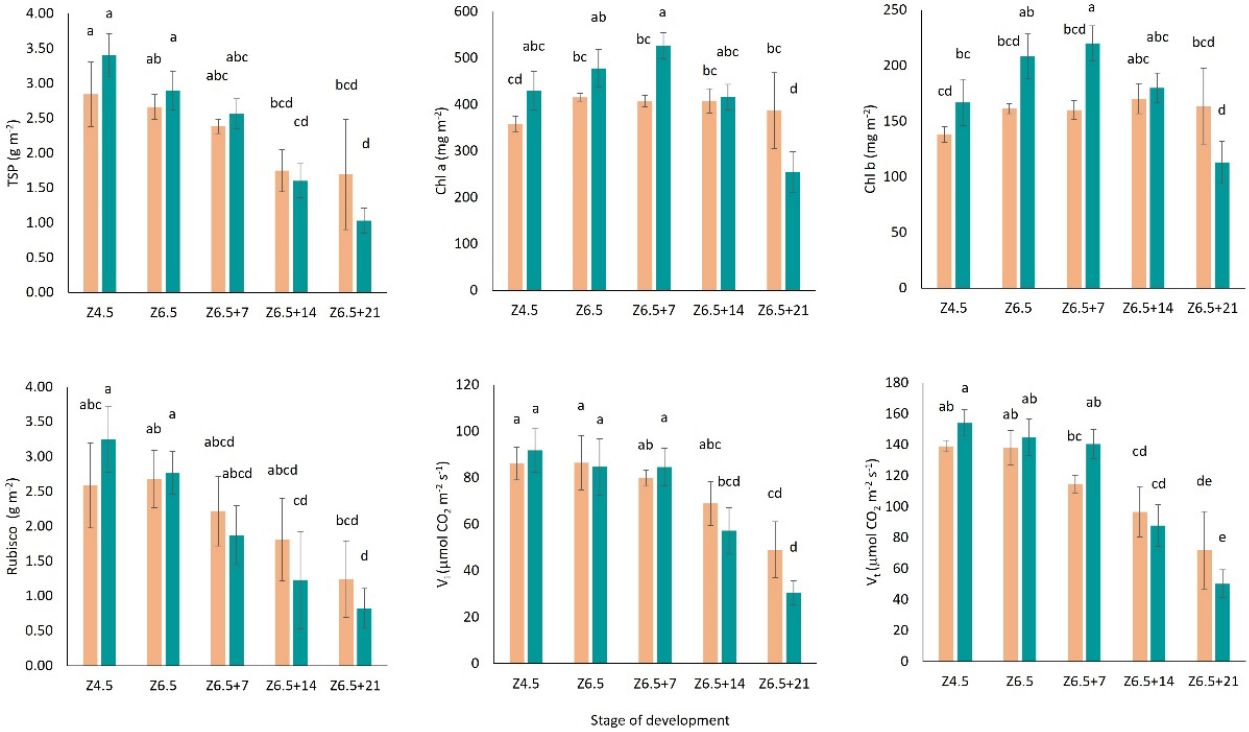

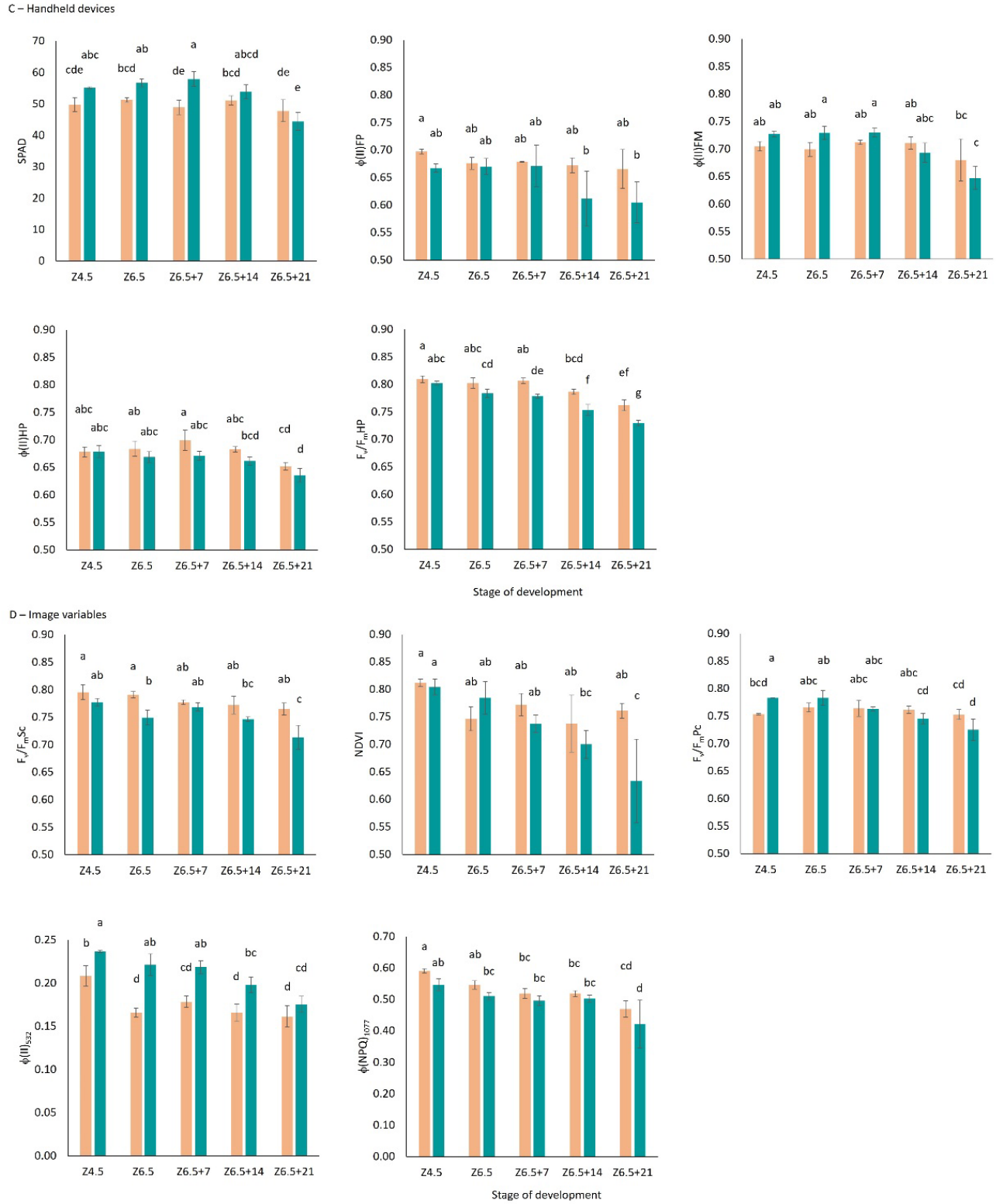

Fig. 3. Mean and standard deviation for each variable for Bobwhite (orange) and Cadenza (blue) at booting (Z4.5), anthesis (Z6.5) and at 7-, 14- and 21-days post anthesis (Z6.5+7, +14, +21) for (A) gas-exchange, (B) biochemical, (C), handheld devices and, (D) image variables. Letters come from the post-hoc test *HSD.test* allowing multiple comparisons of treatments (here time point and cultivar) by means of Tukey. Different letters indicate a statistical difference between cultivar and/or date (a = 0.05).